

# Interpretable Scalar-on-Image Linear Regression Models via the Generalized Dantzig Selector

Sijia Liao

Statistics & Data Science GIDP, University of Arizona

Xiaoxiao Sun \*

Mel and Enid Zuckerman College of Public Health, University of Arizona

Ning Hao

Department of Mathematics, University of Arizona

Hao Helen Zhang

Department of Mathematics, University of Arizona

September 10, 2025

## Abstract

The scalar-on-image regression model examines the association between a scalar response and a bivariate function (e.g., images) through the estimation of a bivariate coefficient function. Existing approaches often impose smoothness constraints to control the bias-variance trade-off, and thus prevent overfitting. However, such assumptions can hinder interpretability, especially when only certain regions of an image influence changes in the response. In such a scenario, interpretability can be better captured by imposing sparsity assumptions on the coefficient function. To address this challenge, we propose the Generalized Dantzig Selector, a novel method that jointly enforces sparsity and smoothness on the coefficient function. The proposed approach enhances interpretability by accurately identifying regions with no contribution to the changes of response, while preserving stability in estimation. Extensive simulation studies and real data applications demonstrate that the new method is highly interpretable and achieves notable improvements over existing approaches. Moreover, we rigorously establish non-asymptotic bounds for the estimation error, providing strong theoretical guarantees for the proposed framework.

*Keywords:* sparse estimation, smoothness regularization, bivariate function, nonparametric regression, non-asymptotic error bound

---

\*Email: xiaosun@arizona.edu.

# 1 INTRODUCTION

In recent years, the *scalar-on-image regression model* has received substantial attention within the statistical research community, catalyzing significant advancements in methodology, theoretical development, and practical applications across diverse fields such as healthcare, neuroscience, and environmental science (Guillas and Lai (2010); Wang et al. (2017); Kang et al. (2018)). This framework is designed to explore the relationship between a scalar response and a bivariate predictor in the form of an image over a spatial domain, providing an interpretable and flexible approach to handling complex data with spatial structures.

Formally, the scalar-on-image linear regression model assumes that we observe a set of paired data  $\{x_i(t, s), y_i\}$  for  $i = 1, 2, \dots, n$ , where each  $x_i(t, s)$  is an image-valued predictor, viewed as a bivariate function defined on the spatial domain  $\Omega = I_t \times I_s$ , with  $I_t, I_s \subseteq \mathbb{R}$  representing intervals on the real line. Correspondingly,  $y_i$  is a scalar-valued response. The relationship between the predictor and the response is modeled as

$$y_i = \alpha + \iint_{\Omega} x_i(t, s) \beta(t, s) dt ds + \epsilon_i, \quad (1)$$

where  $\alpha$  denotes the intercept,  $\beta(t, s)$  is an unknown coefficient function defined over the spatial domain  $I_t \times I_s$ , and  $\epsilon_i$  represents the random error capturing variability unexplained by the model. The function  $\beta(t, s)$  plays a central role in identifying which regions within the image are informative to predicting the response, providing valuable insights for association analysis in real applications. Without loss of generality, throughout this paper we assume  $\Omega = [0, 1] \times [0, 1]$ .

There are several fundamental challenges in scalar-on-image regression. We illustrate these using the hurricane prediction problem as a motivating example. The formation of hurricane in the North Atlantic basin is closely linked to the sea surface temperature

(SST), only in specific geographic regions, as suggested by [Bell and Chelliah \(2006\)](#) and [Saunders and Lea \(2008\)](#). In other words, the influence of SST on hurricane is heterogeneous across the ocean, as shown in Figure 1. Consequently, for a hurricane prediction model, the coefficient estimates for regions that do not influence hurricane formation should ideally be exactly zero to enhance interpretability. At the same time, for regions where the climate influence is non-negligible, enforcing smoothness remains crucial as climate variables such as temperature typically exhibit continuous spatial variation. This dual requirement - sparsity for interpretability and smoothness for stability - highlights the need for refined modeling approaches that can simultaneously address both challenges effectively.

Some of existing techniques emphasize smoothness, such as spline-based approaches ([He and Shi \(1996\)](#); [Ramsay et al. \(2007\)](#); [Crambes et al. \(2009\)](#); [Yuan and Cai \(2010\)](#); [Wood et al. \(2016\)](#); [Wood \(2017\)](#)) and functional principal component analysis methods ([Yao and Lee \(2006\)](#); [Reiss and Ogden \(2007, 2010\)](#); [Goldsmith et al. \(2011\)](#)), and they often produce diffuse and less localized coefficient surfaces, potentially obscuring meaningful spatial patterns. Conversely, methods that prioritize sparsity and feature selection ([Tibshirani \(1996\)](#); [Fan and Li \(2001\)](#); [Candes and Tao \(2007\)](#)) can lead to fragmented or noisy estimates, failing to preserve the spatial coherence that is inherent in many scientific imaging problems. These limitations underscore the need for methodological developments that can seamlessly integrate sparsity and smoothness and thereby produce interpretable and stable estimates of the underlying coefficient function.

In the literature of scalar-on-function regression, there exist methods for incorporating both localized sparsity and smoothness of the coefficient functions, such as [James et al. \(2009\)](#); [Zhou et al. \(2013\)](#); [Lin et al. \(2017\)](#); [Gurer et al. \(2024\)](#) and approaches based on the fused lasso framework ([Tibshirani et al. \(2005\)](#); [Friedman et al. \(2007\)](#)). However, they only focus on univariate functional predictors and can not handle bivariate or multivariate functional

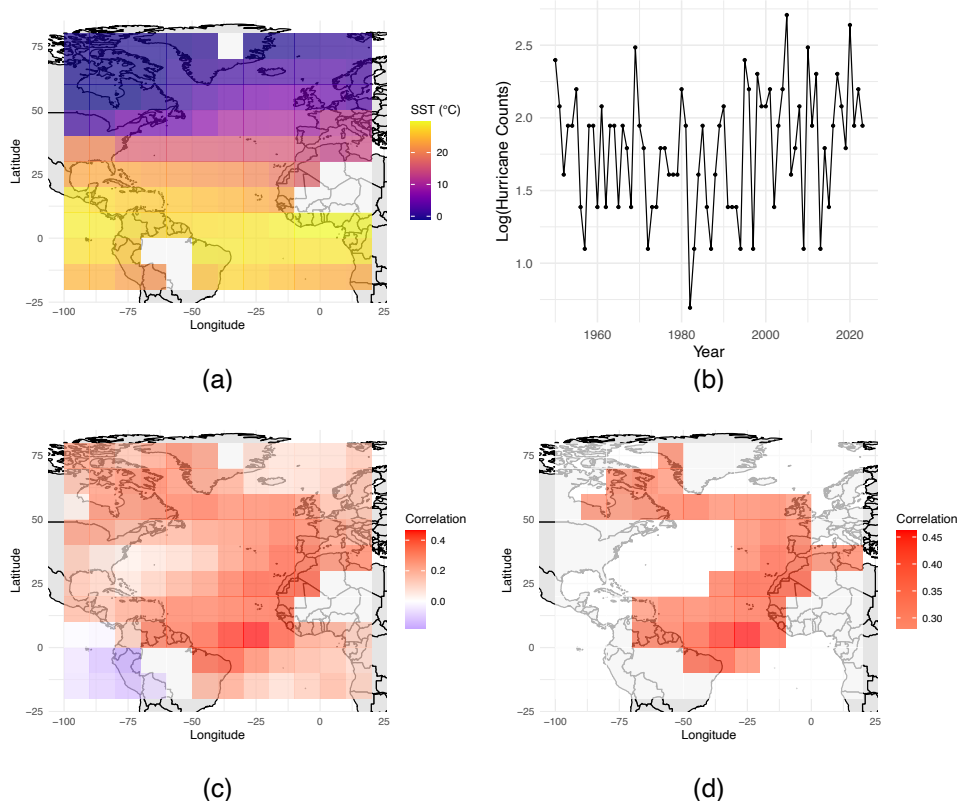


Figure 1: (a) March–April–May averaged Sea Surface Temperature (MAM-SST) in 2023; (b) logarithm of hurricane counts in the North Atlantic basin from 1950 to 2023; (c) correlations between MAM-SST and  $\log(\text{Hurricane Counts})$  over the same period; and (d) statistically significant correlations identified via a Student’s *t*-test with Benjamini–Hochberg adjusted *p*-values at the 0.05 level. The region of interest is  $\Omega = [20^\circ\text{S}, 80^\circ\text{N}] \times [100^\circ\text{W}, 20^\circ\text{E}]$ .

predictors. This gap has motivated us to develop smooth and sparse regression methods for scalar-on-image problems.

In addition, approaches grounded in Bayesian variable selection ([Goldsmith et al. \(2014\)](#); [Li et al. \(2015\)](#); [Kang et al. \(2018\)](#)), while effective in enhancing model interpretability, often entail substantial computational costs and require extensive hyperparameter tuning to achieve satisfactory performance. These limitations can hinder their practical applicability, especially in high-dimensional settings involving complex image data, where scalability and efficiency are critical considerations.

To facilitate interpretation and address existing limitations, we present a new class of scalar-on-image linear models that relate a scalar response to a two-dimensional functional covariate. The proposed Generalized Dantzig Selector (GDS) framework enables the simultaneous enforcement of sparsity and smoothness on the estimated coefficient surface  $\beta(t, s)$  through  $\ell_1$  minimization. To the best of our knowledge, the theoretical properties and applications of such GDS estimators have not been previously explored. The major theoretical contribution of this paper is to establish non-asymptotic error bounds for estimating the coefficient surface under the  $L_2$  norm, as well as for the corresponding predictions measured under the empirical  $n$ -norm.

The new method aims to extend the univariate functional linear regression to the bivariate or even higher-dimensional settings. Such an extension is nontrivial, as it necessitates a unified framework to simultaneously enforcing smoothness along multiple spatial dimensions. Unlike the approach for univariate functional predictors such as [James et al. \(2009\)](#), which employs a classical Dantzig Selector requiring an invertible transformation of the basis expansion, we propose a Generalized Dantzig Selector (GDS) framework that allows for a noninvertible transformation matrix, substantially enhancing the model’s generalizability by flexibly incorporating various smoothness and sparsity constraints. Our approach involves first selecting an appropriate basis representation for the coefficient function, and then minimizing the  $\ell_1$  norm of a linear transformation of the basis coefficients, subject to a constraint on the correlations between predictors and residuals. The design of the linear transformation enables us to approximate both the values of  $\beta(t, s)$  and its directional derivatives on a predefined spatial grid, thereby incorporating localized smoothness into the estimation process. This formulation offers a straightforward yet effective strategy for estimating a sparse and smooth coefficient surface, enhancing both model interpretability and smooth estimation to uncover meaningful relationships between a scalar response and a

bivariate image predictor or higher-dimensional functional predictor.

A notable study by Wang et al. (2017) employs total variation regularization to enforce smoothness while preserving edges in image data. Their approach is limited to using piecewise constant functions to approximate the coefficient surface, with smoothness imposed through bounded total variation. In contrast, our proposed method offers greater flexibility by using various basis representations such as B-splines and incorporating higher-order difference operators to impose different degrees of smoothness. This additional flexibility enables more nuanced control over the smoothness and sparsity of the estimated coefficient surface, facilitating better adaptation to the underlying structural characteristics of image predictors.

The remainder of this paper is organized as follows. Section 2 introduces the necessary notation and presents the methodology underlying our proposed approach. Section 3 provides a theoretical analysis, establishing non-asymptotic error bounds for the estimation and prediction performance of the method. In Section 4, we report simulation results under various settings and compare the proposed method with alternative approaches, including P-splines and functional principal component regression (FPCR). Section 5 illustrates the application of our method to a real-world dataset, where the goal is to predict hurricane counts using the sea surface temperature field. Finally, Section 6 discusses the limitations of the current work and suggests potential directions for future research.

## 2 METHODOLOGY

### 2.1 Notations

Let  $\mathcal{D}_t$  and  $\mathcal{D}_s$  denote the partial derivative operators with respect to  $t$  and  $s$ , respectively.

For  $\alpha_i \in \mathbb{N}$  ( $i = 1, 2$ ), define  $\mathcal{D}^{\alpha_1, \alpha_2} = \mathcal{D}_t^{\alpha_1} \mathcal{D}_s^{\alpha_2}$ .

Let  $L^2(\Omega)$  denote as the space of square-integrable functions defined on a domain  $\Omega$ , i.e.,

$$L^2(\Omega) = \left\{ f : \iint_{\Omega} f^2(t, s) dt ds < \infty \right\}, \text{ and the norm } \|f\|_{L^2(\Omega)} = \left( \iint_{\Omega} f^2(t, s) dt ds \right)^{1/2}.$$

Functions  $f, g \in L^2(\Omega)$  are identified if  $\|f - g\|_{L^2(\Omega)} = 0$ .

For  $d_i \in \mathbb{N}$  ( $i = 1, 2$ ), define

$$L_2^{d_1, d_2}(\Omega) = \left\{ f : \mathcal{D}^{\alpha_1, \alpha_2} f \in L^2(\Omega) \text{ for all } 0 \leq \alpha_1 \leq d_1, 0 \leq \alpha_2 \leq d_2 \right\}.$$

For  $y \in \mathbb{R}^n$ , define the  $n$ -norm

$$\|y\|_n^2 = \frac{1}{n} \sum_{i=1}^n y_i^2.$$

Given  $X \in \mathbb{R}^{n \times p}$ , let

$$D = \text{diag}(\|X_{\cdot 1}\|_n, \dots, \|X_{\cdot p}\|_n)$$

be the diagonal matrix of column  $n$ -norms. Finally, for  $v \in \mathbb{R}^p$ , define

$$\|v\|_{\ell_1} = \sum_{j=1}^p |v_j|, \quad \|v\|_{\ell_2} = \left( \sum_{j=1}^p |v_j|^2 \right)^{1/2}, \quad \|v\|_{\ell_\infty} = \max_{1 \leq j \leq p} |v_j|.$$

## 2.2 Basis Representation

Throughout, we assume that bivariate coefficient function  $\beta(t, s)$  satisfies:

- **Sparsity:** There exists a subset  $\Omega_0 \subset \Omega$  with  $\iint_{\Omega_0} dt ds > 0$  such that  $\beta(t, s) = 0$ , for all  $(t, s) \in \Omega_0$ .
- **Smoothness:** There exist  $d_1, d_2 \in \mathbb{N}$  such that  $\beta \in L_2^{d_1, d_2}(\Omega)$ .

Given a set of basis functions  $\{b_1(t, s), \dots, b_p(t, s)\} \subset L^2(\Omega)$ , let  $\mathcal{V}_p$  denote their span. Then  $\beta(t, s)$  admits the decomposition

$$\beta(t, s) = \mathbf{B}^T(t, s)\eta + e(t, s), \tag{2}$$

where  $\mathbf{B}(t, s) = [b_1(t, s), \dots, b_p(t, s)]^T$ ,  $\eta \in \mathbb{R}^p$  is the coefficient vector, and  $e(t, s)$  captures the approximation error outside  $\mathcal{V}_p$ . Define

$$\eta^* = \arg \min_{\eta \in \mathbb{R}^p} \left( \iint_{\Omega} \left( \beta(t, s) - \mathbf{B}^T(t, s) \eta \right)^2 dt ds \right)^{1/2}.$$

Then  $\beta(t, s) - \mathbf{B}^T(t, s) \eta^*$  lies in the orthogonal complement of  $\mathcal{V}_p$ , and  $\eta^*$  minimizes the  $L_2$  approximation error. For further discussion, let  $\beta^*(t, s) = \mathbf{B}^T(t, s) \eta^*$  and  $\omega_{\mathbf{B}} = \|\beta - \beta^*\|_{L^2(\Omega)}$ . We assume that  $\beta^*(t, s)$  inherits the sparsity and smoothness of  $\beta(t, s)$  under the chosen basis.

A widely used basis for constructing smooth surfaces in multivariate settings is the tensor product B-splines ([Schumaker \(2007\)](#)). This involves selecting knots and spline orders in each dimension to flexibly model underlying structures while mitigating overfitting. Let  $\{\phi_k(t)\}_{k=1}^{p_1}$  and  $\{\psi_l(s)\}_{l=1}^{p_2}$  be B-spline bases of orders  $d_1$  and  $d_2$  with simple knots  $0 < t_1 < \dots < t_{p_1-d_1} < 1$  and  $0 < s_1 < \dots < s_{p_2-d_2} < 1$ , respectively, where  $d_i \in \mathbb{N}$ ,  $p_i \in \mathbb{N}^+$  and  $p_i > d_i$  for  $i = 1, 2$ . A typical tensor product B-spline basis function is

$$b_j(t, s) = \phi_k(t) \psi_l(s), \quad j = (k-1)p_2 + l. \quad (3)$$

Define the maximal knot spacings

$$\Delta_1 = \max_{1 \leq i \leq p_1-d_1-1} |t_i - t_{i+1}|, \quad \Delta_2 = \max_{1 \leq i \leq p_2-d_2-1} |s_i - s_{i+1}|.$$

Theorem 12.7 of [Schumaker \(2007\)](#) (Chapter 12, page 491) shows that there exists  $C > 0$  depending only on  $d_1$  and  $d_2$  such that

$$\omega_{\mathbf{B}} \leq C \left( \Delta_1^{d_1} \|\mathcal{D}_t^{d_1} \beta\|_{L^2(\Omega)} + \Delta_2^{d_2} \|\mathcal{D}_s^{d_2} \beta\|_{L^2(\Omega)} \right)$$

for all  $\beta(t, s) \in L_2^{d_1, d_2}(\Omega)$ .

Another basis often used in practice is the piecewise constant basis, valued for its effectiveness in segmenting the input space into regions with approximately homogeneous properties.



By increasing the number of pieces and incorporating smoothness regulation, one can approximate smooth surfaces while preserving simplicity. Suppose  $p_1, p_2 \in \mathbb{N}^+$ . Let  $I_{t_k} = [t_k, t_{k+1})$  for  $k = 1, \dots, p_1 - 1$  and  $I_{t_{p_1}} = [t_{p_1}, t_{p_1+1}]$ , where  $0 = t_1 < \dots < t_{p_1+1} = 1$ , and similarly define  $I_{s_l} = [s_l, s_{l+1})$  for  $l = 1, \dots, p_2 - 1$  and  $I_{s_{p_2}} = [s_{p_2}, s_{p_2+1}]$ , with  $0 = s_1 < \dots < s_{p_2+1} = 1$ . A piecewise constant basis function is

$$b_j(t, s) = \mathbf{1}\{t \in I_{t_k}, s \in I_{s_l}\}, \quad (4)$$

where  $j = (k - 1)p_2 + l$ ,  $k = 1, \dots, p_1$ , and  $l = 1, \dots, p_2$ . It can be shown that for evenly spaced  $t_1, \dots, t_{p_1+1}$  and  $s_1, \dots, s_{p_2+1}$  in  $[0, 1]$ ,

$$\omega_{\mathbf{B}} \lesssim \frac{1}{\sqrt{p}},$$

for all  $\beta(t, s) \in L^2(\Omega)$ , where  $p = p_1 p_2$  is the total number of pieces.

Define

$$X_{ij} = \iint_{\Omega} x_i(t, s) b_j(t, s) dt ds, \quad \epsilon_i^* = \iint_{\Omega} x_i(t, s) e(t, s) dt ds + \epsilon_i, \quad i = 1, \dots, n,$$

so that (1) can be written as  $y = \alpha + X\eta + \epsilon^*$ . Let

$$\bar{y} = \frac{1}{n} \sum_{i=1}^n y_i, \quad \bar{X} = \frac{1}{n} \sum_{i=1}^n X_i, \quad \bar{\epsilon}^* = \frac{1}{n} \sum_{i=1}^n \epsilon_i^*,$$

where  $X_i$  denotes the  $i$ -th row of  $X$ , and define

$$\tilde{y} = y - \bar{y}, \quad \tilde{X} = X - \mathbf{1}_n \bar{X}, \quad \tilde{\epsilon}^* = \epsilon^* - \bar{\epsilon}^*,$$

with  $\mathbf{1}_n \in \mathbb{R}^n$  the vector of ones. The model can then be centered as  $\tilde{y} = \tilde{X}\eta + \tilde{\epsilon}^*$ .

While one might consider applying variable selection methods to estimate  $\eta$ , sparsity on  $\eta$  generally does not hold for arbitrary bases  $\mathbf{B}^T(t, s)$ , even if  $\beta(t, s)$  is sparse. In Section 2.3, a generalized Dantzig selector is introduced to recover the sparsity and smoothness of  $\beta(t, s)$ . Once an estimator  $\hat{\eta}$  is obtained, the intercept and coefficient function are estimated by

$$\hat{\alpha} = \bar{y} - \bar{X}\hat{\eta}, \quad \hat{\beta}(t, s) = \mathbf{B}^T(t, s)\hat{\eta}.$$

Without loss of generality, we henceforth assume the centered model

$$y = X\eta + \epsilon^*. \quad (5)$$

### 2.3 Proposal: The Generalized Dantzig Selector

The Dantzig selector (Candes and Tao (2007)) estimates sparse coefficients by minimizing the  $\ell_1$  norm under an  $\ell_\infty$  norm constraint on residual correlations. It behaves similarly to the Lasso (Tibshirani (1996); see also Bickel et al. (2009)) and can be efficiently solved via linear programming.

The FLiRTI method (James et al. (2009)) applies the Dantzig selector to finite difference approximations of derivatives in univariate functional regression, relying on an invertible transformation matrix. Our method generalizes FLiRTI to the bivariate setting by introducing a generalized Dantzig selector based on bivariate difference operators, avoiding the impracticality of requiring an invertible transformation matrix.

Let  $\mathbf{I}_m$  denote the  $m \times m$  identity matrix. The  $d$ th order difference matrix for  $v \in \mathbb{R}^m$  is a  $(m - d) \times m$  matrix, denoted by  $\mathbf{D}_m^d$ , with entries

$$\mathbf{D}_m^d(i, j) = \begin{cases} (-1)^k \binom{d}{k}, & \text{if } j = i + k, \quad k = 0, \dots, d, \\ 0, & \text{otherwise.} \end{cases}$$

For example, when  $d = 2$  and  $m = 5$ ,

$$\mathbf{D}_5^2 = \begin{pmatrix} 1 & -2 & 1 & 0 & 0 \\ 0 & 1 & -2 & 1 & 0 \\ 0 & 0 & 1 & -2 & 1 \end{pmatrix}.$$

By convention,  $\mathbf{D}_m^0 = \mathbf{I}_m$ .

Let  $\mathcal{I} = \{(t_k, s_l) \in \Omega : 1 \leq k \leq m_1, 1 \leq l \leq m_2\}$  denote an evenly spaced grid, where a

natural choice is the set of all image pixels. Define the bivariate difference operator

$$A^{d_1, d_2} = \left(\frac{1}{\delta_1}\right)^{d_1} \left(\frac{1}{\delta_2}\right)^{d_2} \mathbf{D}_{m_1}^{d_1} \otimes \mathbf{D}_{m_2}^{d_2},$$

where  $\delta_1, \delta_2$  are the grid lengths in the  $t$  and  $s$  directions and  $\otimes$  denotes the Kronecker product.

Our generalized Dantzig selector solves

$$\begin{aligned} & \min_{\eta \in \mathbb{R}^p} \|A\eta\|_{\ell_1}, \\ \text{subject to } & \left\| \frac{1}{n} D^{-1} X^T (y - X\eta) \right\|_{\ell_\infty} \leq \lambda, \end{aligned} \quad (6)$$

for some  $\lambda > 0$ , where

$$A = \begin{bmatrix} w \mathbf{I}_{m_1 m_2} \\ A^{d_1, d_2} \end{bmatrix} B^T \in \mathbb{R}^{L \times p}, \quad L = m_1 m_2 + (m_1 - d_1)(m_2 - d_2),$$

$w > 0$  controls the sparsity penalty, and  $B$  is the matrix of basis function evaluations at points in  $\mathcal{I}$  such that:

$$B^T = \begin{bmatrix} b_1(t_1, s_1) & \cdots & b_p(t_1, s_1) \\ \vdots & & \vdots \\ b_1(t_{m_1}, s_{m_2}) & \cdots & b_p(t_{m_1}, s_{m_2}) \end{bmatrix}. \quad (7)$$

To separately control smoothness along  $t$  and  $s$ , we extend  $A$  to

$$A = \begin{bmatrix} w \mathbf{I}_{m_1 m_2} \\ A^{d_1, 0} \\ A^{0, d_2} \end{bmatrix} B^T \in \mathbb{R}^{L \times p}, \quad (8)$$

where  $L = m_1 m_2 + (m_1 - d_1)m_2 + m_1(m_2 - d_2)$ ,  $A^{d_1, 0}$  and  $A^{0, d_2}$  are partial difference operators along  $t$  and  $s$ , respectively. The transformation  $A$  links  $\ell_1$  minimization with joint sparsity and smoothness enforcement in  $\beta(t, s)$ . Defining  $\gamma = A\eta$ ,  $\gamma$  approximates a concatenation of  $w\beta(t, s)$ ,  $\mathcal{D}_t^{d_1}\beta(t, s)$ , and  $\mathcal{D}_s^{d_2}\beta(t, s)$  evaluated at  $\mathcal{I}$ .

## 2.4 Computing Algorithm

Let  $\gamma_j^+ = \max\{0, \gamma_j\}$  and  $\gamma_j^- = \max\{0, -\gamma_j\}$  for  $j = 1, \dots, L$ , and similarly define  $\eta_j^+$  and  $\eta_j^-$  for  $j = 1, \dots, p$ . The computation proceeds as follows:

1. Given a grid  $\mathcal{I}$  and data  $\{(x_i(t, s), y_i) : (t, s) \in \mathcal{I}, i = 1, \dots, n\}$ , along with a  $p$ -dimensional basis  $\mathbf{B}$ , orders  $d_1, d_2$ , and sparsity weight  $w$ , construct the basis matrix  $B$ , the design matrix  $X$ , and the transformation matrix  $A$ .
2. Center  $X$  and  $y$ , and compute  $D$ , the diagonal matrix of column  $n$ -norms of the centered  $X$ .
3. For a given  $\lambda > 0$ , solve the following linear program:

$$\begin{aligned}
& \min_{\gamma^+, \gamma^-, \eta^+, \eta^-} \sum_{j=1}^L (\gamma_j^+ + \gamma_j^-) \\
& \text{subject to } A(\eta^+ - \eta^-) = \gamma^+ - \gamma^-, \\
& \quad X^T X(\eta^+ - \eta^-) \leq n\lambda D + X^T y, \\
& \quad -X^T X(\eta^+ - \eta^-) \leq n\lambda D - X^T y, \\
& \quad \gamma^+, \gamma^-, \eta^+, \eta^- \geq 0,
\end{aligned}$$

where all inequalities are interpreted elementwise.

The optimization can be efficiently solved using standard linear programming packages, such as *lpSolve* in *R*.

## 3 THEORETICAL ANALYSIS

### 3.1 Preliminaries

We begin by introducing the necessary notations and definitions.

Define  $f(x_i) = \iint_{\Omega} x_i(t, s) \beta(t, s) dt ds$  for  $i = 1, \dots, n$ , and let  $f = (f(x_1), \dots, f(x_n))^T$ . Similarly, define  $\hat{f}(x_i) = \iint_{\Omega} x_i(t, s) \hat{\beta}(t, s) dt ds$  and  $\hat{f} = (\hat{f}(x_1), \dots, \hat{f}(x_n))^T$ .

In the proposed method, the matrix  $A$  defined in (8) is constructed to have full column rank ( $L \geq p$ ). Suppose  $A$  admits the singular value decomposition (SVD)

$$A = U_1 \begin{bmatrix} \Sigma \\ 0 \end{bmatrix} U_2^T,$$

where  $\Sigma$  is a  $p \times p$  diagonal matrix with singular values in descending order,  $U_1$  and  $U_2$  are unitary matrices. Let

$$A^+ = U_2 [\Sigma^{-1} \mid 0] U_1^T$$

denote the Moore-Penrose pseudoinverse of  $A$ , satisfying  $A^+ A = I_p$ . Define  $V = X A^+$ , so that (5) becomes

$$y = V\gamma + \epsilon^*.$$

Let  $\mathcal{T} \subseteq \{1, \dots, L\}$  be an index set, and let  $V_{\mathcal{T}}$  denote the submatrix of  $V$  consisting of the columns indexed by  $\mathcal{T}$ . We introduce the following definitions related to the identifiability of  $\gamma$  through  $\ell_1$ -minimization and the restricted eigenvalue assumptions, following [Candes and Tao \(2007\)](#) and [Bickel et al. \(2009\)](#).

**Definition 1** ( $S$ -restricted Minimum Eigenvalue). For some integer  $S$  such that  $1 \leq S \leq L$ , the  $S$ -restricted minimum eigenvalue  $\phi_S$  is the largest constant such that

$$\phi_S \|c\|_{\ell_2}^2 \leq \frac{\|V_{\mathcal{T}} c\|_{\ell_2}^2}{n}$$

for all  $\mathcal{T}$  with  $|\mathcal{T}| \leq S$  and all  $c \in \mathbb{R}^{|\mathcal{T}|}$ .

**Definition 2** ( $S, S'$ -restricted Orthogonality Constant). For integers  $S, S'$  such that  $S + S' \leq L$ , the  $S, S'$ -restricted orthogonality constant  $\theta_{S, S'} \geq 0$  is the smallest constant such that

$$\frac{|\langle V_{\mathcal{T}} c, V_{\mathcal{T}'} c' \rangle|}{n} \leq \theta_{S, S'} \|c\|_{\ell_2} \|c'\|_{\ell_2}$$

for all disjoint  $\mathcal{T}, \mathcal{T}'$  with  $|\mathcal{T}| \leq S, |\mathcal{T}'| \leq S'$  and  $c \in \mathbb{R}^{|\mathcal{T}|}, c' \in \mathbb{R}^{|\mathcal{T}'|}$ .

A positive  $\phi_S$  implies that  $V_{\mathcal{T}}$  defines a bijection from  $\mathbb{R}^{|\mathcal{T}|}$  onto its column space for any  $|\mathcal{T}| \leq S$ . A small  $\theta_{S,S'}$  indicates that disjoint subsets of predictors are nearly orthogonal.

For  $h \in \mathbb{R}^L$ , let  $h_{\mathcal{T}}$  denote both the subvector indexed by  $\mathcal{T}$  and, by slight abuse of notation, the vector in  $\mathbb{R}^L$  retaining entries in  $\mathcal{T}$  and setting others to zero.

**Definition 3** (Restricted Eigenvalue I). For some integer  $S$  such that  $1 \leq S \leq L$ , define

$$\kappa_1(S) := \min_{\substack{\mathcal{T}_0 \subset \{1, \dots, L\} \\ |\mathcal{T}_0| \leq S}} \min_{\substack{h \neq 0 \\ \|h_{\mathcal{T}_0^c}\|_{\ell_1} \leq \|h_{\mathcal{T}_0}\|_{\ell_1}}} \frac{\|Vh\|_{\ell_2}}{\sqrt{n} \|h_{\mathcal{T}_0}\|_{\ell_2}}.$$

**Definition 4** (Restricted Eigenvalue II). For integers  $S, S'$  satisfying  $1 \leq S \leq S' \leq L$  and  $S + S' \leq L$ , define

$$\kappa_2(S, S') := \min_{\substack{\mathcal{T}_0 \subset \{1, \dots, L\} \\ |\mathcal{T}_0| \leq S}} \min_{\substack{h \neq 0 \\ \|h_{\mathcal{T}_0^c}\|_{\ell_1} \leq \|h_{\mathcal{T}_0}\|_{\ell_1}}} \frac{\|Vh\|_{\ell_2}}{\sqrt{n} \|h_{\mathcal{T}_{01}}\|_{\ell_2}},$$

where  $\mathcal{T}_1$  is the index set corresponding to the  $S'$  largest (in magnitude) entries of  $h$  outside  $\mathcal{T}_0$ , and  $\mathcal{T}_{01} = \mathcal{T}_0 \cup \mathcal{T}_1$ .

## 3.2 Non-asymptotic Error Bound

In this section, we analyze the non-asymptotic  $L_2$  error bound between  $\hat{\beta}(t, s)$  and the true  $\beta(t, s)$ , as well as the  $n$ -norm error bound between  $\hat{f}$  and  $f$ .

For a given basis  $\mathbf{B}(t, s) = [b_1(t, s), \dots, b_p(t, s)]^\top$ , let  $\eta^*$  and  $\omega_{\mathbf{B}}$  be defined as before, and define  $\gamma^* = A\eta^*$ . Below, we list the technical assumptions used in the subsequent discussions.

**(A1)** The errors are independent Gaussian random variables:

$$\epsilon_i \sim \mathcal{N}(0, \sigma^2), \quad \text{independently for } i = 1, \dots, n, \text{ with } \sigma > 0.$$

**(A2)** The functional covariates are uniformly bounded in the  $L^2(\Omega)$  norm:

$$\|x_i\|_{L^2(\Omega)} \leq M < \infty, \quad \text{for all } i = 1, \dots, n.$$

(A3) The coefficient vector  $\gamma^* \in \mathbb{R}^L$  has at most  $S$  nonzero components.

(A4) The matrix  $V$  satisfies  $\phi_{2S} - \theta_{S,2S} > 0$ .

We are now ready to present the main results of the paper.

**Theorem 1.** *Assume (A1)–(A4) hold. Let  $\hat{\eta}$  be the solution to (6), and define  $\hat{\gamma} = A\hat{\eta}$ .*

*Suppose*

$$\lambda = C\sigma\sqrt{\frac{\log p}{n}} + M\omega_{\mathbf{B}},$$

*for some constant  $C > \sqrt{2}$ . Then, with probability at least  $1 - p^{1-C^2/2}$ ,*

$$\|\hat{\beta} - \beta\|_{L^2(\Omega)} \leq \frac{4C_{\mathbf{B}}\sqrt{L}D_{\max}}{(\phi_{2S} - \theta_{S,2S})\sigma_{\min}^2(A)} \lambda\sqrt{S} + \omega_{\mathbf{B}}, \quad (9)$$

*and*

$$\|\hat{f} - f\|_n \leq \frac{4\sqrt{L}D_{\max}}{\sqrt{\phi_{2S} - \theta_{S,2S}}\sigma_{\min}(A)} \lambda\sqrt{S} + M\omega_{\mathbf{B}}, \quad (10)$$

*where  $\hat{\beta}(t, s) = \mathbf{B}^T(t, s)\hat{\eta}$ ,  $C_{\mathbf{B}} = \left(\sum_{j=1}^p \iint_{\Omega} b_j^2(t, s) dt ds\right)^{1/2}$ ,  $D_{\max} = \max_{j=1, \dots, p} D_j$ , and  $\sigma_{\min}(A)$  is the smallest singular value of  $A$ .*

*Remark* (Comparison with [Candes and Tao \(2007\)](#)). The condition  $1 - \delta_{2S} > \theta_{S,2S}$  used in [Candes and Tao \(2007\)](#) guarantees identifiability of  $\gamma$ , where  $\delta_S$  is the  $S$ -restricted isometry constant (see also [Candes and Tao \(2005\)](#)). Specifically,  $\delta_S$  is the smallest constant such that

$$(1 - \delta_S)\|c\|_{\ell_2}^2 \leq \frac{\|V_{\mathcal{T}}c\|_{\ell_2}^2}{n} \leq (1 + \delta_S)\|c\|_{\ell_2}^2$$

for all  $|\mathcal{T}| \leq S$ . Here in (A4), we adopt the alternative condition  $\phi_{2S} > \theta_{S,2S}$ , which avoids requiring an upper bound on the restricted eigenvalues of  $V^T V/n$  while still ensuring the proof to proceed.

However, the condition (A4) is generally difficult to verify and may not hold for arbitrary design matrices. In Theorem 2, we relax this requirement by adopting a restricted eigenvalue

condition, following a similar approach to that in [Bickel et al. \(2009\)](#). Below, we list the restricted eigenvalue conditions.

**(A5)** The matrix  $V$  satisfies the restricted eigenvalue condition  $\kappa_1(S) > 0$ .

**(A6)** The matrix  $V$  satisfies the stronger restricted eigenvalue condition  $\kappa_2(S, S) > 0$ .

We note that condition **(A4)** serves as a sufficient condition for both **(A5)** and **(A6)**, and that **(A6)** further implies **(A5)**. For additional discussion, we refer the reader to the supplementary material and [Bickel et al. \(2009\)](#). Our main result, Theorem 2, requires only one of the weaker conditions—either **(A5)** or **(A6)**—leading to slightly different bounds depending on the assumption adopted.

**Theorem 2.** *Assume **(A1)**–**(A3)** and **(A5)** hold. Let  $\hat{\eta}$  be the solution to (6), and define  $\hat{\gamma} = A\hat{\eta}$ . Suppose*

$$\lambda = C\sigma\sqrt{\frac{\log p}{n}} + M\omega_{\mathbf{B}},$$

*for some constant  $C > \sqrt{2}$ . Then, with probability at least  $1 - p^{1-C^2/2}$ ,*

$$\|\hat{\beta} - \beta\|_{L^2(\Omega)} \leq \frac{8C_{\mathbf{B}}\sqrt{L}D_{\max}}{\kappa_1^2(S)\sigma_{\min}^2(A)} \lambda S + \omega_{\mathbf{B}}, \quad (11)$$

*and*

$$\|\hat{f} - f\|_n \leq \frac{4\sqrt{L}D_{\max}}{\kappa_1(S)\sigma_{\min}(A)} \lambda\sqrt{S} + M\omega_{\mathbf{B}}, \quad (12)$$

*with the same definitions of  $\hat{\beta}(t, s)$ ,  $C_{\mathbf{B}}$ ,  $D_{\max}$ , and  $\sigma_{\min}(A)$  as in Theorem 1.*

*If, in addition, **(A6)** holds, then with the same probability,*

$$\|\hat{\beta} - \beta\|_{L^2(\Omega)} \leq \frac{8C_{\mathbf{B}}\sqrt{L}D_{\max}}{\kappa_2^2(S, S)\sigma_{\min}^2(A)} \lambda\sqrt{S} + \omega_{\mathbf{B}}. \quad (13)$$

*Remark (Interpretation of the Bound).* Let  $\beta^*(t, s) = \mathbf{B}^T(t, s)\eta^*$  denote the “oracle” approximation under basis  $\mathbf{B}$ . Then

$$\|\hat{\beta} - \beta\|_{L^2(\Omega)} \leq \|\hat{\beta} - \beta^*\|_{L^2(\Omega)} + \|\beta^* - \beta\|_{L^2(\Omega)},$$



where  $\|\beta^* - \beta\|_{L^2(\Omega)} = \omega_{\mathbf{B}}$  is fixed given  $\mathbf{B}$ . The bound on  $\|\hat{\beta} - \beta^*\|_{L^2(\Omega)}$  depends on  $\lambda$ , which itself depends on  $\omega_{\mathbf{B}}$ . In practice, to achieve good approximation, especially with piecewise constant bases,  $p$  should be chosen large enough so that  $M\omega_{\mathbf{B}}$  is dominated by  $C\sigma\sqrt{(\log p)/n}$ .

Several constants appearing in Theorems 1 and 2 merit further discussion. Among them, the quantities  $\phi_{2S} - \theta_{S,2S}$ ,  $\kappa_1(S)$ , and  $\kappa_2(S, S)$  depend on the sparsity level  $S$ , the design matrix  $X$ , and the transformation matrix  $A$ . However, these terms are generally intractable and cannot be computed in closed form. To provide some intuition, we include a simple illustrative example in the supplementary material where assumptions **(A5)** and **(A6)** are not numerically violated, and we provide the estimates of  $\kappa_1(S)$  and  $\kappa_2(S, S)$  in that setting. In contrast, the other constants in the bounds are more transparent and can be readily computed. Specifically,  $D_{\max}$  depends only on the covariates  $X$ ,  $C_{\mathbf{B}}$  is determined solely by the choice of basis functions  $\mathbf{B}$ , and both  $L$  and  $\sigma_{\min}(A)$  rely only on the transformation matrix  $A$ .

Given the basis matrix  $B^T$  defined in (7), it is possible to choose the weight  $w$  to make  $\sqrt{L}/\sigma_{\min}(A)$  a constant. For example, using the piecewise constant basis defined in (4), and aligning the estimation grid in (8) with the partitioning (i.e., one grid point per piece),  $B^T$  becomes the identity matrix, yielding  $C_{\mathbf{B}} = 1$  and  $\sigma_{\min}(A) = w$ . Moreover, setting  $w = \sqrt{L}$  ensures  $\sqrt{L}/\sigma_{\min}(A) = 1$ , leading to the simplified bound in (13)

$$\|\hat{\beta} - \beta\|_{L^2(\Omega)} \leq \frac{8D_{\max}}{\kappa_2^2(S, S)} \lambda \sqrt{\frac{S}{L}} + \omega_{\mathbf{B}}.$$

Here,  $S/L$  can be roughly interpreted as the average area proportion of the nonzero regions of  $\beta(t, s)$ ,  $\mathcal{D}_t^{d_1}\beta(t, s)$ , and  $\mathcal{D}_s^{d_2}\beta(t, s)$  within  $\Omega$  (if the partial derivatives exist).

Although a larger  $w$  increases  $\sigma_{\min}(A)$ , it does not necessarily improve estimation. On one hand,  $w$  rescales  $A$  and thus affects  $\kappa_2(S, S)$ . On the other hand, an extremely large  $w$  may

lead to an overly sparse estimate, sacrificing smoothness. In practice, we recommend setting  $w$  to some positive constants, or selecting  $w$  via cross-validation.

## 4 SIMULATION STUDY

### 4.1 Evaluations

To evaluate the performance of the proposed method and competing approaches under different settings, we compute the Mean Squared Error (MSE)

$$\text{MSE} = \frac{1}{n} \sum_{i=1}^n (\hat{f}(x_i) - y_i)^2$$

on an independent test set of size 10,000.

In addition to MSE, we consider the Relative Integrated Squared Error (RISE) of  $\hat{\beta}$ ,

$$\text{RISE}(\hat{\beta}) = \frac{\iint_{\Omega} (\hat{\beta}(t, s) - \beta(t, s))^2 dt ds}{\iint_{\Omega} \beta^2(t, s) dt ds},$$

as well as the recovery rates of the zero and nonzero regions, defined respectively as

$$R_1(\hat{\beta}) = \frac{\iint_{\Omega} I_{\{|\hat{\beta}(t,s)|=0\} \cap \{|\beta(t,s)|=0\}}(t, s) dt ds}{\iint_{\Omega} I_{\{|\beta(t,s)|=0\}}(t, s) dt ds},$$

and

$$R_2(\hat{\beta}) = \frac{\iint_{\Omega} I_{\{|\hat{\beta}(t,s)|>0\} \cap \{|\beta(t,s)|>0\}}(t, s) dt ds}{\iint_{\Omega} I_{\{|\beta(t,s)|>0\}}(t, s) dt ds}.$$

These metrics collectively assess both the prediction accuracy and the ability to recover the true sparsity structure of the coefficient function  $\beta(t, s)$ .

### 4.2 Parameter Tuning

The proposed method involves tuning  $d_1$ ,  $d_2$ ,  $w$ , and  $\lambda$  to balance sparsity, smoothness, and prediction. The orders  $d_1$  and  $d_2$  (controlling smoothness) can be selected from candidate grids (e.g.,  $\{0, 1, 2, 3\}$ ) and the sparsity weight  $w$  can be set based on the instruction in

section 3.2. The tuning parameter  $\lambda$ , regulating both fit and sparsity, is recommended to vary proportionally to  $\sqrt{\log p/n}$ .

Parameter selection may be performed via information criteria (such as AIC and BIC) when model simplicity is prioritized. Under piecewise constant bases, aligning the estimation grid with basis pieces allows the degrees of freedom to be defined as the size of active set  $\mathcal{A}(\hat{\eta}) = \{j : \hat{\eta}_j \neq 0\}$ . Such information criteria works well when the sample size is large, but may lead to suboptimal selection in small samples; cross-validation is then preferred.

### 4.3 A Refitting Step

Large  $\lambda$  values, especially when selected by information criteria, can introduce bias. To correct this, one may apply a refitting step, regulating smoothness only over the active set where  $\hat{\beta}(t, s) \neq 0$ , similar to the Gauss-Dantzig Selector (Candes and Tao (2007)).

Given  $\hat{\eta}$  from (6), define

$$\hat{\mathcal{I}}_0 = \{(t, s) \in \mathcal{I} : \mathbf{B}^T(t, s)\hat{\eta} = 0\},$$

and solve

$$\min_{\eta \in \mathbb{R}^p} \|A\eta\|_{\ell_1}, \quad \text{subject to} \quad \left\| \frac{1}{n} D^{-1} X^T (y - X\eta) \right\|_{\ell_\infty} \leq \lambda \quad \text{and} \quad B_{\hat{\mathcal{I}}_0}^T \eta = 0.$$

Here,  $w = 0$  is set in  $A$  to avoid additional shrinkage, and  $\lambda$  is re-tuned via cross-validation.

### 4.4 Simulation Settings

In the simulations, data were generated from the following  $\beta$  surfaces:

- $\beta_1(t, s) = \phi(t)\phi(s)$ , where  $\phi(t) = \sin(\pi t) - \sin(\pi/4)$  for  $t \in [0, 1/4]$ ,  $\phi(t) = \sin(3\pi/4) - \sin(\pi t)$  for  $t \in [3/4, 1]$ , and  $\phi(t) = 0$  otherwise.
- $\beta_2(t, s) = \phi(t)\phi(s)$ , where  $\phi(t) = 100 (\exp(t - 0.5)^2 - \exp(0.04))$  for  $t \in [0.3, 0.7]$ , and  $\phi(t) = 0$  otherwise.

- $\beta_3(t, s)$  is piecewise defined:  $200((t - 0.6)^2 + (s - 0.4)^2 - 0.04)$  if  $(t - 0.6)^2 + (s - 0.4)^2 \leq 0.04$ ;  $200(0.04 - (t - 0.4)^2 - (s - 0.6)^2)$  if  $(t - 0.4)^2 + (s - 0.6)^2 \leq 0.04$ ; and 0 otherwise.

The true  $\beta$  surfaces are shown in the leftmost column of Figure 2.

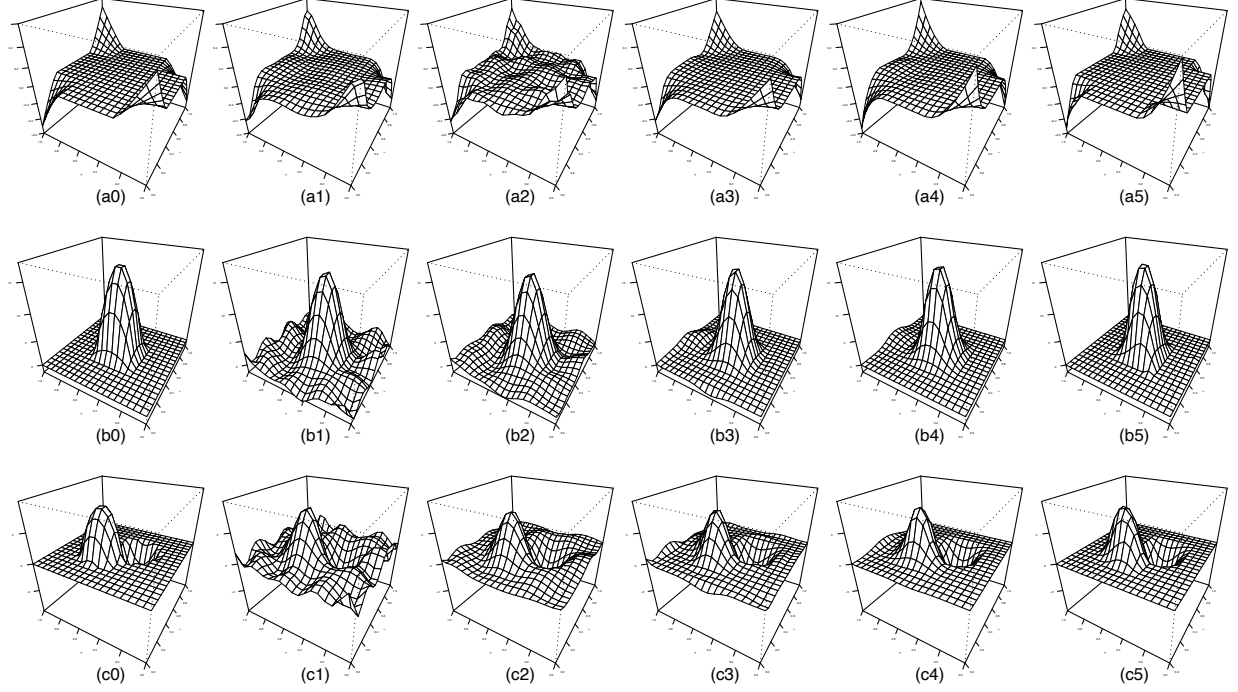


Figure 2: True coefficient surfaces  $\beta$  (a0–c0) and fitted surfaces  $\hat{\beta}$  under predictor  $P_1$  by P-splines (a1–c1), FPCR (a2–c2), and the proposed methods:  $\text{GDS}_{B_1}$  (a3–c3),  $\text{GDS}_{B_2}$  (a4–c4), and  $\text{GDS}_{B_2, \text{AIC, Re}}$  (a5–c5).

Each predictor surface was generated as

$$x(t, s) = \sum_{k=1}^m \sum_{j=1}^m a_{jk} \psi_j(t) \psi_k(s),$$

where  $a_{jk} \sim \mathcal{N}(0, 1)$  independently for  $j, k = 1, \dots, m$ , and  $\{\psi_j(t)\}_{j=1}^m$  denotes a set of basis functions. We considered the following basis settings:

$P_1$ : B-splines of order 4 with 6 interior knots evenly spaced on  $[0, 1]$ , yielding  $m = 10$ .

$P_2$ : B-splines of order 5 with 15 interior knots evenly spaced on  $[0, 1]$ , yielding  $m = 20$ .

All combinations  $(\beta_j, P_k)$  for  $j = 1, 2, 3$  and  $k = 1, 2$  were evaluated.

Random noise was generated from  $\mathcal{N}(0, \sigma^2)$  to achieve a signal-to-noise ratio

$$\text{SNR}(\sigma) = \frac{\text{Var}(\iint_{\Omega} x_i(t, s)\beta(t, s) dt ds)}{\text{Var}(\epsilon_i)}$$

equal to 4. All integrals were approximated via Gaussian quadrature with equal weights at the grid points  $\mathcal{I}$  with  $m_1 \times m_2 = 400$ . Experiments were conducted with a training sample size of  $n = 400$  (unless specified otherwise), comparing the proposed method with the penalized B-splines (P-splines; see [Wood \(2017\)](#)) and functional principal components regression (FPCR; see [Reiss and Ogden \(2007\)](#)).

Let  $B_1$  denote the tensor-product B-spline basis defined in (3), with 7 interior knots and order 3 in each direction, and  $B_2$  denote the piecewise constant basis defined in (4) with  $p_1 = p_2 = 20$ . We set the difference operator orders to  $d_1 = d_2 = 2$  for  $B_1$  and  $d_1 = d_2 = 3$  for  $B_2$ , producing locally quadratic-like surfaces. The tuning parameters in the proposed method were  $\lambda$  and  $w$ , and the corresponding method using  $B_1$  and  $B_2$  were denoted as  $\text{GDS}_{B_1}$  and  $\text{GDS}_{B_2}$ , respectively.

The P-splines method was fitted using  $B_1$ , with the smoothing parameter selected via an independent validation set of the same size as the training data. For FPCR, the number of components was chosen to capture 100*pve*% of the variance, where *pve* was selected from 0.90, 0.91, ..., 0.99 by the same validation set, while other parameters were set following [Reiss and Ogden \(2007\)](#). The parameters in  $\text{GDS}_{B_1}$  and  $\text{GDS}_{B_2}$  were tuned using the same validation set as for the P-splines and FPCR methods. Additionally,  $\text{GDS}_{B_2}$  was tuned using AIC, with the corresponding post-refitted results denoted as  $\text{GDS}_{B_2, \text{AIC}, \text{Re}}$ . Refitting was applied only when AIC was used, and only the post-refitted results are reported in Section 4.5.

## 4.5 Results

The models were fitted using the selected tuning parameters and the mean squared errors (MSEs) were evaluated on an independent test set. This procedure was repeated 100 times to compute the average MSEs and their standard errors, with results summarized in Table 1.

To further assess coefficient estimation and interpretability, we calculated the average relative integrated squared errors (RISEs) of  $\hat{\beta}$ , the average zero region recovery rates ( $R_1(\hat{\beta})$ ), the average nonzero region recovery rates ( $R_2(\hat{\beta})$ ), and their corresponding standard errors. These results are reported in Tables 2, 3, and 4.

Method	$\beta_1 (10^{-6})$		$\beta_2 (10^{-2})$		$\beta_3 (10^{-2})$	
	$P_1$	$P_2$	$P_1$	$P_2$	$P_1$	$P_2$
P-splines	10.15 (0.01)	5.39 (0.01)	3.48 (0.005)	1.01 (0.001)	1.03 (0.002)	0.38 (0.001)
FPCR	10.68 (0.02)	5.41 (0.01)	3.35 (0.004)	0.98 (0.001)	0.98 (0.001)	0.37 (0.001)
GDS $_{B_1}$	<b>9.96 (0.01)</b>	<b>5.13 (0.01)</b>	3.19 (0.004)	<b>0.90 (0.001)</b>	0.94 (0.001)	<b>0.34 (0.001)</b>
GDS $_{B_2}$	9.99 (0.01)	5.29 (0.01)	3.18 (0.004)	0.92 (0.001)	0.93 (0.001)	0.35 (0.001)
GDS $_{B_2, \text{AIC, Re}}$	<b>9.97 (0.01)</b>	5.20 (0.01)	<b>3.13 (0.004)</b>	<b>0.89 (0.001)</b>	<b>0.91 (0.001)</b>	<b>0.33 (0.001)</b>

Table 1: Mean squared errors (MSEs) (in indicated units) and standard errors (in parentheses) across methods and settings.

In terms of both prediction accuracy and  $\beta$  estimation, the proposed methods GDS $_{B_1}$  and GDS $_{B_2}$  consistently outperform P-splines and FPCR across all settings. Although GDS $_{B_2, \text{AIC, Re}}$  shows suboptimal performance under limited sample sizes for the  $\beta_1$  setting, its performance improves substantially as the sample size increases, as illustrated in Figures 3 and 4.

The mean values of  $R_1(\hat{\beta})$  and  $R_2(\hat{\beta})$  in Tables 3 and 4 were computed by truncating  $\hat{\beta}(t, s)$  to zero where its absolute value was smaller than  $10^{-8}$ . It is evident that the P-splines and FPCR methods fail to identify zero and nonzero regions under any setting. In contrast, the

Method	$\beta_1$		$\beta_2$		$\beta_3$	
	$P_1$	$P_2$	$P_1$	$P_2$	$P_1$	$P_2$
P-splines	2.71 (0.02)	3.85 (0.03)	12.37 (0.11)	6.67 (0.05)	15.08 (0.11)	9.42 (0.06)
FPCR	6.79 (0.09)	3.59 (0.04)	7.29 (0.06)	5.52 (0.04)	8.16 (0.06)	7.13 (0.05)
GDS $_{B_1}$	<b>1.96 (0.03)</b>	<b>2.15 (0.03)</b>	2.63 (0.05)	<b>1.70 (0.02)</b>	4.60 (0.04)	4.33 (0.03)
GDS $_{B_2}$	2.10 (0.02)	3.02 (0.04)	3.10 (0.05)	2.92 (0.04)	5.04 (0.06)	5.09 (0.05)
GDS $_{B_2, \text{AIC, Re}}$	2.80 (0.07)	3.03 (0.07)	<b>2.33 (0.08)</b>	<b>1.71 (0.05)</b>	<b>4.11 (0.05)</b>	<b>3.67 (0.04)</b>

Table 2: Mean relative integrated squared errors (RISEs) (in units of  $10^{-2}$ ) and standard errors (in parentheses) across methods and settings.

Method	$\beta_1$		$\beta_2$		$\beta_3$	
	$P_1$	$P_2$	$P_1$	$P_2$	$P_1$	$P_2$
P-splines	0.00 (0.00)	0.00 (0.00)	0.00 (0.00)	0.00 (0.00)	0.00 (0.00)	0.00 (0.00)
FPCR	0.00 (0.00)	0.00 (0.00)	0.00 (0.00)	0.00 (0.00)	0.00 (0.00)	0.00 (0.00)
GDS $_{B_1}$	5.25 (0.25)	3.84 (0.21)	23.16 (0.34)	36.03 (0.79)	26.20 (0.50)	21.69 (0.44)
GDS $_{B_2}$	9.40 (0.66)	5.31 (0.35)	56.92 (1.12)	44.24 (1.04)	55.92 (1.01)	36.42 (0.92)
GDS $_{B_2, \text{AIC, Re}}$	<b>93.94 (0.22)</b>	<b>89.58 (0.39)</b>	<b>99.07 (0.07)</b>	<b>97.88 (0.13)</b>	<b>93.04 (0.12)</b>	<b>92.11 (0.18)</b>

Table 3: Mean  $R_1(\hat{\beta})$  values (percentage of correctly identified zero regions) and standard errors (in parentheses) across methods and settings.

proposed method using the piecewise constant basis (GDS $_{B_2}$ ) identifies over 30% of the true zero regions while maintaining more than 99% precision in identifying nonzero regions for  $\beta_2$  and  $\beta_3$ . Moreover, the AIC-tuned version (GDS $_{B_2, \text{AIC, Re}}$ ) successfully recovers over 89% of the true zero regions across all settings, while achieving over 91% precision for the nonzero regions.

Figure 2 displays the estimated  $\beta$  surfaces from various methods under predictor  $P_1$ , alongside the true surface. While the P-splines and FPCR methods produce bumpy estimates, the proposed methods clearly recover the flat zero regions in  $\beta_1$ ,  $\beta_2$ , and  $\beta_3$ , providing

Method	$\beta_1$		$\beta_2$		$\beta_3$	
	$P_1$	$P_2$	$P_1$	$P_2$	$P_1$	$P_2$
P-splines	100.00 (0.00)	100.00 (0.00)	100.00 (0.00)	100.00 (0.00)	100.00 (0.00)	100.00 (0.00)
FPCR	100.00 (0.00)	100.00 (0.00)	100.00 (0.00)	100.00 (0.00)	100.00 (0.00)	100.00 (0.00)
GDS $_{B_1}$	99.89 (0.02)	99.94 (0.01)	99.97 (0.01)	100.00 (0.00)	99.99 (0.01)	99.99 (0.01)
GDS $_{B_2}$	99.92 (0.02)	99.82 (0.02)	99.94 (0.02)	99.77 (0.03)	99.76 (0.04)	99.88 (0.02)
GDS $_{B_2, \text{AIC, Re}}$	93.63 (0.26)	91.44 (0.31)	97.41 (0.37)	98.33 (0.11)	96.30 (0.20)	95.91 (0.18)

Table 4: Mean  $R_2(\hat{\beta})$  values (percentage of correctly identified nonzero regions) and standard errors (in parentheses) across methods and settings.

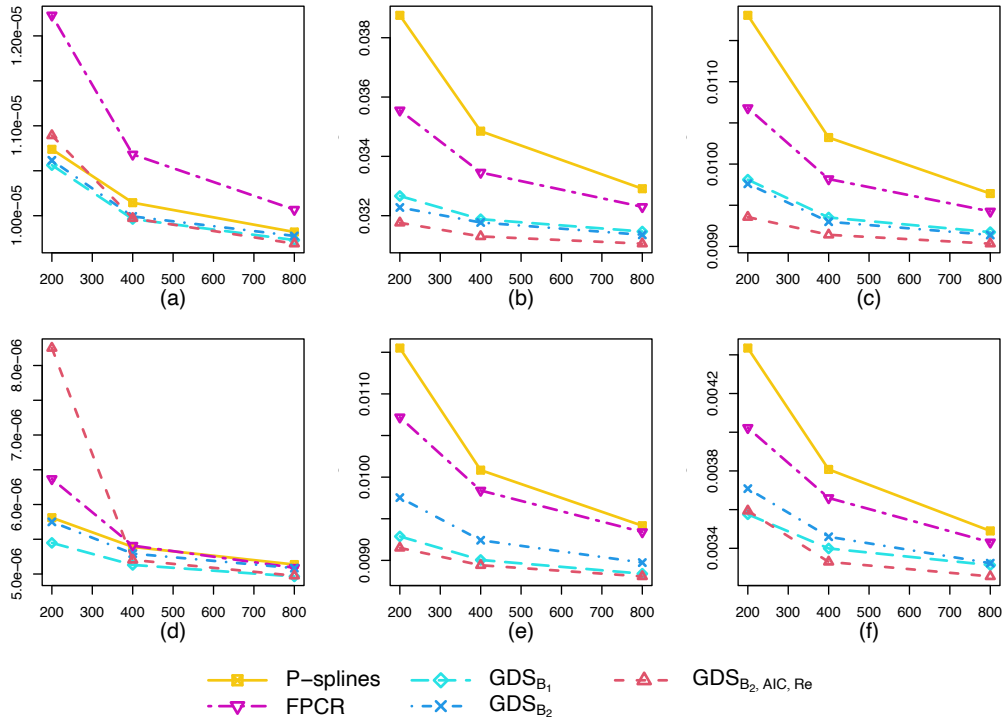


Figure 3: Mean squared errors (MSEs) versus sample size (200, 400, 800) across predictor settings ( $P_1$ : panels a-c;  $P_2$ : panels d-f) and coefficient settings ( $\beta_1$ : panels a, d;  $\beta_2$ : panels b, e;  $\beta_3$ : panels c, f).

interpretable insights into the shape and localization of predictive versus non-predictive regions. These findings align with the theoretical results in Section 3 and demonstrate



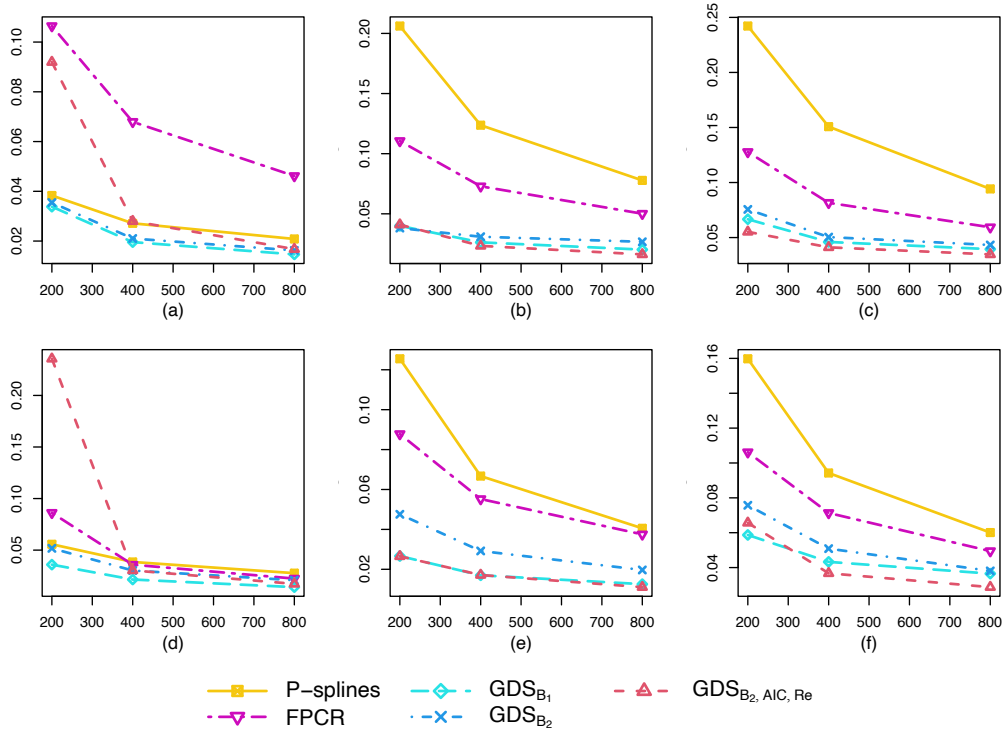


Figure 4: Mean relative integrated squared errors (RISEs) versus sample size (200, 400, 800) across predictor settings ( $P_1$ : panels a–c;  $P_2$ : panels d–f) and coefficient settings ( $\beta_1$ : panels a, d;  $\beta_2$ : panels b, e;  $\beta_3$ : panels c, f).

that the proposed method effectively yields smooth, interpretable coefficient surfaces while accurately distinguishing between relevant and irrelevant regions.

## 5 REAL DATA STUDY

Hurricane activity is widely recognized to be influenced by several large-scale environmental factors, including sea surface temperatures (SSTs), the El Niño–Southern Oscillation (ENSO), sea level pressure (SLP), the Atlantic Multidecadal Oscillation (AMO), and vertical wind shear, among others. Established frameworks for studying and predicting hurricane activity include models developed by NOAA’s Climate Prediction Center (CPC) (Bell and Chelliah (2006)), the Tropical Storm Risk (TSR) consortium (Saunders and Lea (2008)), and Colorado

State University (CSU) (Klotzbach and Gray (2009); Klotzbach et al. (2017)). These models primarily focus on forecasting seasonal metrics, such as the total number of hurricanes. Among environmental predictors, SSTs are considered particularly critical, with many models (Bell and Chelliah (2006); Vimont and Kossin (2007); Saunders and Lea (2008); Klotzbach and Gray (2009); Davis et al. (2015)) leveraging SSTs from subtropical or tropical regions to improve prediction accuracy.

The UA model proposed in Davis et al. (2015) employs models a linear relationship between the logarithm of hurricane counts and environmental predictors, including SSTs. Specifically, it uses the average SSTs from March to May within the region  $0^{\circ}$ – $20^{\circ}$ N and  $60^{\circ}$ W– $10^{\circ}$ E to construct a scalar SST predictor. This model provides a simple yet effective approach for forecasting hurricane counts in the North Atlantic Basin.

We extend the analysis by applying our proposed method to investigate the relationship between hurricane counts and SSTs in the North Atlantic Basin, while enhancing interpretability through spatial variability. To focus on SST effects, we consider a simplified model assuming consistent hurricane patterns over the years and excluding other predictors, with the region of interest defined as  $\Omega = [20^{\circ}\text{S}, 80^{\circ}\text{N}] \times [100^{\circ}\text{W}, 20^{\circ}\text{E}]$ .

The problem is formulated by the scalar-on-image model in (1), where  $y_i$  denotes the logarithm of hurricane counts in year  $i$ , and  $x_i(t, s)$  represents the March–April–May averaged SST (MAM-SST) at location  $(t, s)$ . Since SSTs are defined only over ocean surfaces, the integral is effectively restricted to the sea surface within  $\Omega$ . The values of  $x_i(t, s)$  were set to zero over land, which does not affect the model, as land regions contribute nothing to the integral.

Sea surface temperature data were obtained from the Extended Reconstructed Sea Surface Temperature version 5 (ERSSTv5) dataset Huang et al. (2017), and historical hurricane counts for the North Atlantic basin were accessed via the International Best Track Archive

for Climate Stewardship (IBTrACS) [Knapp et al. \(2010\)](#); [Gahtan et al. \(2024\)](#). Data from 1950 to 2004 were used for training, and data from 2005 to 2023 were reserved for testing, resulting in a training-to-testing split of approximately 3:1. For simplicity, the domain  $\Omega$  was partitioned into  $10^\circ \times 10^\circ$  grids, and the region-averaged MAM-SST values were used as predictors; see Figure 1. Integrals over  $\Omega$  were computed using Gaussian quadrature, with weights proportional to the relative area of each region.

In the proposed method, we set  $d_1 = d_2 = d$  and used  $B_1$  (cubic B-splines with six degrees of freedom in each direction) and  $B_2$  (with  $p_1 = 12$  and  $p_2 = 10$ ) for modeling. For the P-splines method, the same  $B_1$  basis was employed. For the FPCR method, the number of basis functions in each direction was set to six, with the default penalty order of two. Model parameters— $(d, w, \lambda)$  for  $\text{GDS}_{B_1}$  and  $\text{GDS}_{B_2}$ , the smoothing parameter for P-splines, and the proportion of variance explained ( $pve$ ) for FPCR—were selected via 10-fold cross-validation. The trained models were then used to predict the logarithm of hurricane counts on the test set.

The performance of each method was evaluated by computing the root mean squared error (RMSE,  $(\sum_{i=1}^n (\hat{y}_i - y_i)^2 / n)^{1/2}$ ) and mean absolute error (MAE,  $\sum_{i=1}^n |\hat{y}_i - y_i| / n$ ) on the test set, as summarized in Table 5. Predictions issued in June by Colorado State University (CSU) were also included for comparison. The CSU forecasts rely on four predictors: (i) ECMWF-predicted September SSTs in the equatorial Pacific (issued on May 1), (ii) April–May SSTs in the eastern North Atlantic, (iii) April–May 200-mb zonal winds in the tropical Pacific, and (iv) May sea level pressure in the central North Atlantic. Historical CSU forecasts are available at <https://tropical.colostate.edu/archive.html>. Despite relying solely on MAM-SSTs, the  $\text{GDS}_{B_2}$  method achieves a 10.3% reduction in RMSE and an 11.6% reduction in MAE compared to CSU’s June predictions.

Figure 5 shows that the estimated  $\beta$  surface from proposed methods effectively captures

	P-splines	FPCR	GDS <sub>B<sub>1</sub></sub>	GDS <sub>B<sub>2</sub></sub>	CSU
RMSE	0.412	0.421	0.409	0.401	0.447
MAE	0.328	0.317	0.313	0.311	0.352

Table 5: Root mean squared errors (RMSEs) and mean absolute errors (MAEs) for predictions from 2005 to 2023.

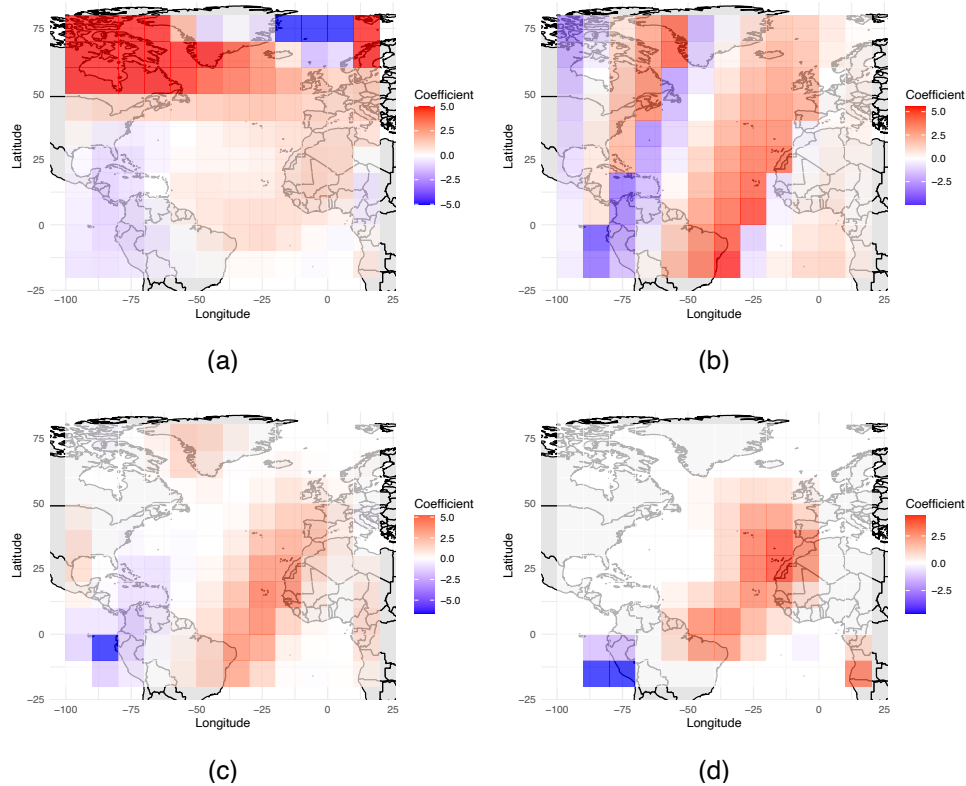


Figure 5: Estimated coefficient surfaces from (a) P-splines, (b) FPCR, (c) GDS<sub>B<sub>1</sub></sub>, and (d) GDS<sub>B<sub>2</sub></sub>. Extreme values of  $\hat{\beta}$  in (a) are truncated for visualization purposes.

the regions where correlations between MAM-SSTs and the logarithm of hurricane counts are significant at the 0.05 level. These regions closely align with findings reported by [Bell and Chelliah \(2006\)](#), [Vimont and Kossin \(2007\)](#), [Saunders and Lea \(2008\)](#), and [Davis et al. \(2015\)](#). Figure 6 presents the test set predictions from each method, along with the corresponding 95% bootstrapped confidence intervals (shaded), the observed hurricane

counts on the log scale, and CSU’s June forecasts on the log scale.

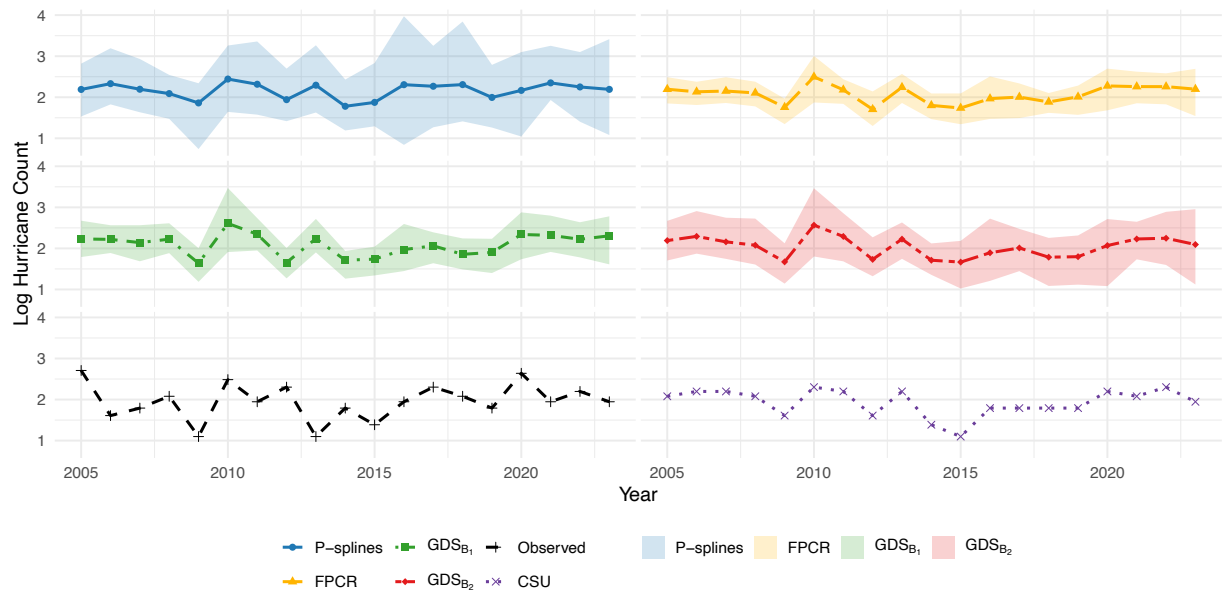


Figure 6: Predictions from 2005 to 2023 with 95% bootstrapped confidence intervals, compared with observed hurricane counts and CSU’s June forecasts on the log scale.

## 6 DISCUSSION

We have developed the Generalized Dantzig Selector (GDS) method for estimating the coefficient function in scalar-on-image regression models via a basis expansion framework. Additionally, we have provided a non-asymptotic theoretical analysis of our estimator, establishing finite-sample error bounds under mild conditions. Results from both simulation studies and real-world data applications demonstrate that our method effectively produces a smooth and interpretable coefficient surface while accurately recovering zero (non-predictive) and nonzero (predictive) regions.

While our current work focuses on models with a single image predictor, several directions for future research remain. One promising extension is to accommodate models involving multiple image-based predictors or multimodal data, where spatial information from different

sources may jointly influence the response. Another important direction is to generalize the framework to broader classes of scalar-on-image models, such as those with non-Gaussian outcomes or generalized linear model (GLM) structures. These extensions would further enhance the flexibility and applicability of the GDS approach in modern high-dimensional imaging studies.

## ACKNOWLEDGMENTS

Funding was provided in part by R21AR083495-01A1, R01AR080742-02S1, and UA Eighteenth Mile TRIF Funding.

## DISCLOSURE STATEMENT

The authors report there are no competing interests to declare.

## SUPPLEMENTARY MATERIAL

**Proofs.** Proofs of all lemmas and theorems are provided in the online supplementary material.

**Code and Data.** The SST data are available from the [NOAA](#), and the raw hurricane data can be accessed from the [IBTrACS](#).

## References

- Bell, G. D. and Chelliah, M. (2006); ‘Leading tropical modes associated with interannual and multidecadal fluctuations in north atlantic hurricane activity’; Journal of Climate **19**(4), 590–612.
- Bickel, P. J., Ritov, Y. and Tsybakov, A. B. (2009); ‘Simultaneous analysis of Lasso and

Dantzig selector’; The Annals of Statistics **37**(4), 1705–1732.

**URL:** <https://doi.org/10.1214/08-AOS620>

Candes, E. J. and Tao, T. (2005); ‘Decoding by linear programming’; IEEE transactions on information theory **51**(12), 4203–4215.

Candes, E., Rudelson, M., Tao, T. and Vershynin, R. (2005); Error correction via linear programming; in ‘46th Annual IEEE Symposium on Foundations of Computer Science (FOCS’05)’; pp. 668–681.

Candes, E. and Tao, T. (2007); ‘The Dantzig selector: Statistical estimation when  $p$  is much larger than  $n$ ’; The Annals of Statistics **35**(6), 2313–2351.

**URL:** <https://doi.org/10.1214/009053606000001523>

Crambes, C., Kneip, A. and Sarda, P. (2009); ‘Smoothing splines estimators for functional linear regression’; The Annals of Statistics **37**(1), 35–72.

**URL:** <https://doi.org/10.1214/07-AOS563>

Davis, K., Zeng, X. and Ritchie, E. A. (2015); ‘A new statistical model for predicting seasonal north atlantic hurricane activity’; Weather and Forecasting **30**(3), 730–741.

Donoho, D. and Huo, X. (2001); ‘Uncertainty principles and ideal atomic decomposition’; IEEE Transactions on Information Theory **47**(7), 2845–2862.

Fan, J. and Li, R. (2001); ‘Variable selection via nonconcave penalized likelihood and its oracle properties’; Journal of the American statistical Association **96**(456), 1348–1360.

Friedman, J., Hastie, T., Höfling, H. and Tibshirani, R. (2007); ‘Pathwise coordinate optimization’; The Annals of Applied Statistics **1**(2), 302–332.

**URL:** <https://doi.org/10.1214/07-AOAS131>

Gahtan, J., Knapp, K. R., Schreck, C. J. I., Diamond, H. J., Kossin, J. P. and Kruk, M. C.

(2024); ‘International best track archive for climate stewardship (ibtracs) project, version 4.01’. [ibtracs.NA.list.v04r01.csv], accessed on November 9, 2024.

**URL:** <https://doi.org/10.25921/82ty-9e16>

Goldsmith, J., Bobb, J., Crainiceanu, C. M., Caffo, B. and Reich, D. (2011); ‘Penalized functional regression’; Journal of computational and graphical statistics **20**(4), 830–851.

Goldsmith, J., Huang, L. and Crainiceanu, C. M. (2014); ‘Smooth scalar-on-image regression via spatial bayesian variable selection’; Journal of Computational and Graphical Statistics **23**(1), 46–64.

Guillas, S. and Lai, M.-J. (2010); ‘Bivariate splines for spatial functional regression models’; Journal of Nonparametric Statistics **22**(4), 477–497.

**URL:** <https://doi.org/10.1080/10485250903323180>

Gurer, S., Shang, H. L., Mandal, A. and Beyaztas, U. (2024); ‘Locally sparse and robust partial least squares in scalar-on-function regression’; Statistics and Computing **34**(5), 150.

He, X. and Shi, P. (1996); ‘Bivariate tensor-product b-splines in a partly linear model’; Journal of Multivariate Analysis **58**(2), 162–181.

Huang, B., Thorne, P. W., Banzon, V. F., Boyer, T., Chepurin, G., Lawrimore, J. H., Menne, M. J., Smith, T. M., Vose, R. S. and Zhang, H.-M. (2017); ‘Extended reconstructed sea surface temperature, version 5 (ersstv5): Upgrades, validations, and intercomparisons’; Journal of Climate **30**(20), 8179–8205. [sst.mnmean.nc], accessed on October 25, 2024.

**URL:** <https://journals.ametsoc.org/view/journals/clim/30/20/jcli-d-16-0836.1.xml>

James, G. M., Wang, J. and Zhu, J. (2009); ‘Functional linear regression that’s interpretable’; The Annals of Statistics **37**(5A), 2083–2108.

**URL:** <https://doi.org/10.1214/08-AOS641>

Kang, J., Reich, B. J. and Staicu, A.-M. (2018); ‘Scalar-on-image regression via the soft-



thresholded Gaussian process'; Biometrika **105**(1), 165–184.

**URL:** <https://doi.org/10.1093/biomet/asx075>

Klotzbach, P. J. and Gray, W. M. (2009); 'Twenty-five years of atlantic basin seasonal hurricane forecasts (1984–2008)'; Geophysical research letters **36**(9).

Klotzbach, P. J., Saunders, M. A., Bell, G. D. and Blake, E. S. (2017); 'North atlantic seasonal hurricane prediction: underlying science and an evaluation of statistical models'; Climate extremes: Patterns and mechanisms pp. 315–328.

Knapp, K. R., Kruk, M. C., Levinson, D. H., Diamond, H. J. and Neumann, C. J. (2010); 'The international best track archive for climate stewardship (ibtracs): Unifying tropical cyclone data'; Bulletin of the American Meteorological Society **91**(3), 363–376.

**URL:** [https://journals.ametsoc.org/view/journals/bams/91/3/2009bams2755\\_1.xml](https://journals.ametsoc.org/view/journals/bams/91/3/2009bams2755_1.xml)

Li, F., Zhang, T., Wang, Q., Gonzalez, M. Z., Maresh, E. L. and Coan, J. A. (2015); 'Spatial bayesian variable selection and grouping for high-dimensional scalar-on-image regression'; The Annals of Applied Statistics **9**(2).

**URL:** <http://dx.doi.org/10.1214/15-AOAS818>

Lin, Z., Cao, J., Wang, L. and Wang, H. (2017); 'Locally sparse estimator for functional linear regression models'; Journal of Computational and Graphical Statistics **26**(2), 306–318.

Ramsay, J. O., Hooker, G., Campbell, D. and Cao, J. (2007); 'Parameter Estimation for Differential Equations: a Generalized Smoothing Approach'; Journal of the Royal Statistical Society Series B: Statistical Methodology **69**(5), 741–796.

**URL:** <https://doi.org/10.1111/j.1467-9868.2007.00610.x>

Reiss, P. T. and Ogden, R. T. (2007); 'Functional principal component regression and functional partial least squares'; Journal of the American Statistical Association **102**(479), 984–996.

- Reiss, P. T. and Ogden, R. T. (2010); ‘Functional generalized linear models with images as predictors’; Biometrics **66**(1), 61–69.
- Saunders, M. A. and Lea, A. S. (2008); ‘Large contribution of sea surface warming to recent increase in atlantic hurricane activity’; Nature **451**(7178), 557–560.
- Schumaker, L. (2007); Spline functions: basic theory; Cambridge university press.
- Tibshirani, R. (1996); ‘Regression shrinkage and selection via the lasso’; Journal of the Royal Statistical Society Series B: Statistical Methodology **58**(1), 267–288.
- Tibshirani, R., Saunders, M., Rosset, S., Zhu, J. and Knight, K. (2005); ‘Sparsity and smoothness via the fused lasso’; Journal of the Royal Statistical Society Series B: Statistical Methodology **67**(1), 91–108.
- Vimont, D. J. and Kossin, J. P. (2007); ‘The atlantic meridional mode and hurricane activity’; Geophysical Research Letters **34**(7).
- URL:** <https://agupubs.onlinelibrary.wiley.com/doi/abs/10.1029/2007GL029683>
- Wang, X., Zhu, H. and Initiative, A. D. N. (2017); ‘Generalized scalar-on-image regression models via total variation’; Journal of the American Statistical Association **112**(519), 1156–1168.
- Wood, S. N. (2017); ‘P-splines with derivative based penalties and tensor product smoothing of unevenly distributed data’; Statistics and Computing **27**, 985–989.
- Wood, S. N., Pya, N. and Säfken, B. (2016); ‘Smoothing parameter and model selection for general smooth models’; Journal of the American Statistical Association **111**(516), 1548–1563.
- Yao, F. and Lee, T. C. (2006); ‘Penalized spline models for functional principal compo-

nent analysis'; Journal of the Royal Statistical Society Series B: Statistical Methodology **68**(1), 3–25.

Yuan, M. and Cai, T. T. (2010); 'A reproducing kernel Hilbert space approach to functional linear regression'; The Annals of Statistics **38**(6), 3412–3444.

**URL:** <https://doi.org/10.1214/09-AOS772>

Zhou, J., Wang, N.-Y. and Wang, N. (2013); 'Functional linear model with zero-value coefficient function at sub-regions'; Statistica Sinica **23**, 25–50.

## SUPPLEMENTARY MATERIAL

This supplementary material provides the detailed proofs of Theorems 1 and 2 from the main article, along with additional discussions on the restricted eigenvalue conditions.

### 7 Proof of Theorem 1

Before presenting the proof of Theorem 1, we introduce several technical lemmas, namely Lemmas 1–6. Among these, Lemmas 1–3 also play a key role in the proof of Theorem 2. Lemmas 4 and 5 are slight modifications of Lemma 3.1 and related results in Candes and Tao (2007). Complete proofs for all lemmas are provided.

#### 7.1 Lemma 1

Lemma 1 applies generally to the basis representation introduced in (2). It also holds under the orthogonal decomposition of  $\beta$ , where  $\eta$  is replaced by  $\eta^*$  and  $\omega$  by  $\omega_{\mathbf{B}}$ .

**Lemma 1.** *Suppose  $\epsilon_i \sim \mathcal{N}(0, \sigma^2)$  independently for  $i = 1, \dots, n$ , with  $\sigma > 0$ , and assume there exists a constant  $M < \infty$  such that  $\|x_i\|_{L^2(\Omega)} \leq M$  for all  $i$ . Let  $\eta$  denote the coefficient vector under the selected basis  $\mathbf{B}$  as defined in (2), and let  $\omega = \|e\|_{L^2(\Omega)}$ . Set*

$$\lambda = C\sigma\sqrt{\frac{\log p}{n}} + M\omega,$$

for some constant  $C > \sqrt{2}$ . Then, with probability at least  $1 - p^{1-C^2/2}$ ,

$$\left\| \frac{1}{n} D^{-1} X^\top (y - X\eta) \right\|_{\ell_\infty} \leq \lambda.$$

*Proof of Lemma 1.* We aim to determine the value of  $\lambda$  such that  $\left\| \frac{1}{n} D^{-1} X^\top (y - X\eta) \right\|_{\ell_\infty} \leq \lambda$  holds with high probability. Define

$$v_i = \int_0^1 \int_0^1 x_i(t, s) e(t, s) dt ds, \tag{14}$$

for  $i = 1, \dots, n$ , and let  $v = (v_1, \dots, v_n)^T$ . Then we have

$$\begin{aligned} \frac{1}{n} D^{-1} X^T (y - X\eta) &= \frac{1}{n} D^{-1} X^T \epsilon^* \\ &= \frac{1}{n} D^{-1} X^T \epsilon + \frac{1}{n} D^{-1} X^T v. \end{aligned}$$

The  $j$ th element of  $\frac{1}{n} D^{-1} X^T (y - X\eta)$  is given by

$$\left( \frac{1}{n} D^{-1} X^T (y - X\eta) \right)_j = \frac{1}{n} D_j^{-1} X_j^T \epsilon + \frac{1}{n} D_j^{-1} X_j^T v.$$

Note that  $D_j = \sqrt{\frac{1}{n} \sum_{i=1}^n X_{ij}^2}$ . The expression above can be rewritten as

$$\left( \frac{1}{n} D^{-1} X^T (y - X\eta) \right)_j = \frac{1}{\sqrt{n}} \tilde{X}_j^T \epsilon + \frac{1}{\sqrt{n}} \tilde{X}_j^T v, \quad (15)$$

where  $\tilde{X}_j = X_j / \sqrt{\sum_{i=1}^n X_{ij}^2}$ , for  $j = 1, \dots, p$ . Notice that  $\|\tilde{X}_j\|_{\ell_2} = 1$ . It follows that

$$\tilde{X}_j^T \epsilon \sim N(0, \sigma^2)$$

and

$$|\tilde{X}_j^T v| \leq \|\tilde{X}_j\|_{\ell_2} \|v\|_{\ell_2} = \|v\|_{\ell_2}.$$

Now we bound the second term in (15). Since  $|v_i| \leq \|x_i\|_{L^2(\Omega)} \|e\|_{L^2(\Omega)} \leq M\omega$  for each  $i = 1, \dots, n$ , and  $\|v\|_{\ell_2} \leq \sqrt{n} \|v\|_{\ell_1}$ , we have

$$\left| \frac{1}{\sqrt{n}} \tilde{X}_j^T v \right| \leq \|v\|_{\ell_1} \leq M\omega, \quad \text{for all } j = 1, \dots, p.$$

To bound the first term in (15), note that for  $Z \sim N(0, \sigma^2)$  and any  $t \geq 0$ , we have

$$\begin{aligned} P(Z \geq t) \exp \left\{ \frac{t^2}{2\sigma^2} \right\} &= \int_t^\infty \frac{1}{\sqrt{2\pi}\sigma} \exp \left\{ -\frac{x^2}{2\sigma^2} \right\} dx \cdot \exp \left\{ \frac{t^2}{2\sigma^2} \right\} \\ &= \int_t^\infty \frac{1}{\sqrt{2\pi}\sigma} \exp \left\{ -\frac{(x-t)^2}{2\sigma^2} \right\} \exp \left\{ \frac{2t^2 - 2xt}{2\sigma^2} \right\} dx \\ &\leq \int_t^\infty \frac{1}{\sqrt{2\pi}\sigma} \exp \left\{ -\frac{(x-t)^2}{2\sigma^2} \right\} dx \\ &\leq \frac{1}{2}. \end{aligned}$$

Therefore,  $P(|Z| \geq t) \leq 2P(Z \geq t) \leq \exp\left\{-\frac{t^2}{2\sigma^2}\right\}$  for any  $t \geq 0$ .

Let  $Z_j = \tilde{X}_j^T \epsilon$ , then  $Z_j \sim N(0, \sigma^2)$  for  $j = 1, \dots, p$ . Furthermore,

$$\begin{aligned} P\left(\sup_j |Z_j| \geq t\right) &= P\left(\bigcup_{j=1}^p \{|Z_j| \geq t\}\right) \\ &\leq \sum_{j=1}^p P(|Z_j| \geq t) \\ &\leq p \exp\left\{-\frac{t^2}{2\sigma^2}\right\}. \end{aligned}$$

Setting  $t = C\sigma\sqrt{\log p}$  gives

$$P\left(\sup_j |Z_j| \geq C\sigma\sqrt{\log p}\right) \leq p \exp\left\{-\frac{C^2 \log p}{2}\right\} = p^{1-C^2/2}.$$

Therefore, for any  $C > \sqrt{2}$ , with probability at least  $1 - p^{1-C^2/2}$ , we have

$$\sup_j \left| \frac{1}{\sqrt{n}} \tilde{X}_j^T \epsilon \right| \leq C\sigma\sqrt{\frac{\log p}{n}}.$$

Combining the above with (15), we conclude that

$$\begin{aligned} \left\| \frac{1}{n} D^{-1} X^T (y - X\eta) \right\|_{\ell_\infty} &\leq \sup_j \left| \frac{1}{\sqrt{n}} \tilde{X}_j^T \epsilon \right| + \sup_j \left| \frac{1}{\sqrt{n}} \tilde{X}_j^T v \right| \\ &\leq C\sigma\sqrt{\frac{\log p}{n}} + M\omega, \end{aligned}$$

with probability at least  $1 - p^{1-C^2/2}$  for any  $C > \sqrt{2}$ . This completes the proof.  $\square$

## 7.2 Lemma 2

**Lemma 2.** *Let  $\gamma = A\eta$ . Suppose  $\gamma$  has at most  $S$  nonzero components, and let  $\mathcal{T}_0 = \{j : \gamma_j \neq 0\}$  denote its true support. If*

$$\left\| \frac{1}{n} D^{-1} X^T (y - X\eta) \right\|_{\ell_\infty} \leq \lambda,$$

*then for  $\hat{\eta}$  obtained as the solution to (6), defining  $h = \hat{\gamma} - \gamma$  with  $\hat{\gamma} = A\hat{\eta}$  and letting  $\mathcal{T}_1$  be the  $S$  largest entries of  $h$  outside  $\mathcal{T}_0$ , we have*

$$\|h_{\mathcal{T}_0^c}\|_{\ell_2} \leq \frac{1}{\sqrt{S}} \|h_{\mathcal{T}_0^c}\|_{\ell_1}, \quad (16)$$

where  $\mathcal{T}_{01} = \mathcal{T}_0 \cup \mathcal{T}_1$ , and

$$\|h_{\mathcal{T}_0^c}\|_{\ell_1} \leq \|h_{\mathcal{T}_0}\|_{\ell_1}. \quad (17)$$

*Proof of Lemma 2.* Following the argument in [Candes and Tao \(2007\)](#), we first observe that the  $k$ th largest entry of  $h_{\mathcal{T}_0^c}$  satisfies

$$k \cdot |h_{\mathcal{T}_0^c}|_{(k)} \leq \|h_{\mathcal{T}_0^c}\|_{\ell_1},$$

which implies

$$\|h_{\mathcal{T}_{01}^c}\|_{\ell_2}^2 = \sum_{k \geq S+1} |h_{\mathcal{T}_0^c}|_{(k)}^2 \leq \|h_{\mathcal{T}_0^c}\|_{\ell_1}^2 \sum_{k \geq S+1} \frac{1}{k^2} \leq \frac{1}{S} \|h_{\mathcal{T}_0^c}\|_{\ell_1}^2,$$

establishing (16).

Next, since both  $\hat{\gamma}$  and  $\eta$  are feasible solutions to problem (6), it follows that

$$\|\hat{\gamma}\|_{\ell_1} \leq \|\gamma\|_{\ell_1}.$$

As shown similarly in [Candes and Tao \(2007\)](#) and [Donoho and Huo \(2001\)](#), this implies

$$\|h_{\mathcal{T}_0^c}\|_{\ell_1} \leq \|h_{\mathcal{T}_0}\|_{\ell_1}.$$

To prove this, decompose  $\hat{\gamma} = \gamma + h$ , and note that

$$\|\gamma + h\|_{\ell_1} - \|\gamma\|_{\ell_1} = \|h_{\mathcal{T}_0^c}\|_{\ell_1} + \|(\gamma + h)_{\mathcal{T}_0}\|_{\ell_1} - \|\gamma_{\mathcal{T}_0}\|_{\ell_1} \leq 0.$$

Rewriting the above yields

$$\begin{aligned} \|h_{\mathcal{T}_0^c}\|_{\ell_1} + \|\gamma_{\mathcal{T}_0}\|_{\ell_1} - \|h_{\mathcal{T}_0}\|_{\ell_1} &\leq \|h_{\mathcal{T}_0^c}\|_{\ell_1} + \|(\gamma + h)_{\mathcal{T}_0}\|_{\ell_1} \\ &\leq \|\gamma_{\mathcal{T}_0}\|_{\ell_1}, \end{aligned}$$

which implies

$$\|h_{\mathcal{T}_0^c}\|_{\ell_1} \leq \|h_{\mathcal{T}_0}\|_{\ell_1}.$$

This concludes the proof of (17). □

### 7.3 Lemma 3

**Lemma 3.** *Let  $V = XA^+$  and  $\gamma^* = A\eta^*$ . The model (6) is equivalent to the following optimization problem*

$$\min_{\gamma \in \mathbb{R}^L} \|\gamma\|_{\ell_1}, \quad \text{subject to} \quad \left\| \frac{1}{n} D^{-1} X^\top (y - V\gamma) \right\|_{\ell_\infty} \leq \lambda.$$

*Let  $\hat{\gamma}$  be the solution to it and suppose that  $\gamma^*$  is also a feasible solution. Then the difference  $h = \hat{\gamma} - \gamma^*$  satisfies*

$$\frac{1}{n} \|V^\top V h\|_{\ell_\infty} \leq \frac{\sqrt{L} D_{\max}}{\sigma_{\min}(A)} \left\| \frac{1}{n} D^{-1} X^\top V h \right\|_{\ell_\infty}. \quad (18)$$

*Proof of Lemma 3.* By construction, the matrix  $A \in \mathbb{R}^{L \times p}$ , where  $L \geq p$ , and there exists a pseudo-inverse  $A^+ \in \mathbb{R}^{p \times L}$  such that  $A^+ A = I_p$ . Recall that  $y = V\gamma + \epsilon^*$ , where  $V = XA^+$  and  $\gamma = A\eta$ . Solving the optimization problem defined in (6) is equivalent to obtaining  $\hat{\gamma}$  by solving

$$\min_{\gamma \in \mathbb{R}^L} \|\gamma\|_{\ell_1}, \quad \text{subject to} \quad \left\| \frac{1}{n} D^{-1} X^\top (y - V\gamma) \right\|_{\ell_\infty} \leq \lambda.$$

Let  $h = \hat{\gamma} - \gamma^*$ . Since both  $\hat{\gamma}$  and  $\gamma^*$  are feasible, it follows from the triangle inequality that

$$\left\| \frac{1}{n} D^{-1} X^\top V h \right\|_{\ell_\infty} \leq 2\lambda. \quad (19)$$

Let  $\mathcal{T}_0 = \{j : \gamma_j^* \neq 0\}$  be the support of  $\gamma^*$ , with  $|\mathcal{T}_0| \leq S$ . Let  $\mathcal{T}_1$  be the indices of the  $S$  largest entries of  $h$  outside  $\mathcal{T}_0$ , and define  $\mathcal{T}_{01} = \mathcal{T}_0 \cup \mathcal{T}_1$ . From Lemma 2, we know

$$\|h_{\mathcal{T}_0^c}\|_{\ell_1} \leq \|h_{\mathcal{T}_0}\|_{\ell_1}.$$

Next, we have

$$\|V^\top V h\|_{\ell_\infty} = \|A^{+\top} X^\top V h\|_{\ell_\infty} \leq \|DA^+\|_1 \left\| D^{-1} X^\top V h \right\|_{\ell_\infty},$$

where the inequality follows from  $\|Mv\|_{\ell_\infty} \leq \|M\|_\infty \|v\|_{\ell_\infty}$  and  $\|M^\top\|_\infty = \|M\|_1$ . Here,  $\|\cdot\|_\infty$ ,  $\|\cdot\|_1$ , and  $\|\cdot\|_2$  denote matrix/operator norms.



Moreover,

$$\|DA^+\|_1 \leq D_{\max}\|A^+\|_1, \quad \text{and} \quad \|A^+\|_1 \leq \sqrt{L}\|A^+\|_2 = \frac{\sqrt{L}}{\sigma_{\min}(A)},$$

where the last equality uses the singular value decomposition of  $A$ . Therefore,

$$\frac{1}{n}\|V^\top Vh\|_{\ell_\infty} \leq \frac{\sqrt{L}D_{\max}}{\sigma_{\min}(A)} \left\| \frac{1}{n}D^{-1}X^\top Vh \right\|_{\ell_\infty},$$

which establishes (18).  $\square$

## 7.4 Lemma 4

**Lemma 4** (cf. Lemma 3.1 in Candes and Tao (2007)). *Let  $\mathcal{T}_0$  be an index set with  $|\mathcal{T}_0| = S$ , where  $3S \leq L$ . Suppose  $V \in \mathbb{R}^{n \times L}$  satisfies  $\phi_{2S} > \theta_{S,2S}$ . For any  $h \in \mathbb{R}^L$ , let  $\mathcal{T}_1$  denote the set of the  $S$  largest entries of  $h$  outside of  $\mathcal{T}_0$ , and set  $\mathcal{T}_{01} = \mathcal{T}_0 \cup \mathcal{T}_1$ . Then*

$$\|h_{\mathcal{T}_{01}}\|_{\ell_2} \leq \frac{1}{n\phi_{2S}}\|V_{\mathcal{T}_{01}}^T Vh\|_{\ell_2} + \frac{\theta_{S,2S}}{\phi_{2S}S^{1/2}}\|h_{\mathcal{T}_0^c}\|_{\ell_1}.$$

*Proof of Lemma 4.* Consider the restricted transformation

$$V_{\mathcal{T}_{01}} : \mathbb{R}^{|\mathcal{T}_{01}|} \rightarrow \mathbb{R}^n, \quad V_{\mathcal{T}_{01}} c_{\mathcal{T}_{01}} := \sum_{j \in \mathcal{T}_{01}} c_j V^j.$$

Let  $\mathcal{W} \subset \mathbb{R}^n$  denote the span of  $\{V^j : j \in \mathcal{T}_{01}\}$ . Then  $\mathcal{W}$  is the range of  $V_{\mathcal{T}_{01}}$  and the orthogonal complement of the kernel of  $V_{\mathcal{T}_{01}}^T$ . Thus,  $\mathbb{R}^n = \mathcal{W} \oplus \mathcal{W}^\perp$ .

Since  $\phi_{2S} > 0$ , we know that  $V_{\mathcal{T}_{01}}$  is a bijection from  $\mathbb{R}^{|\mathcal{T}_{01}|}$  to  $\mathcal{W}$ , with singular values greater than or equal to  $\sqrt{n\phi_{2S}}$ . By Definition 1, for any  $c \in \mathbb{R}^L$ , we have

$$\sqrt{\phi_{2S}}\|c_{\mathcal{T}_{01}}\|_{\ell_2} \leq \|V_{\mathcal{T}_{01}} c_{\mathcal{T}_{01}}\|_{\ell_2} / \sqrt{n}.$$

Let  $P_{\mathcal{W}}$  denote the orthogonal projection onto  $\mathcal{W}$ . For each  $v \in \mathbb{R}^n$ , we have  $V_{\mathcal{T}_{01}}^T v = V_{\mathcal{T}_{01}}^T P_{\mathcal{W}} v$ .

Since  $V_{\mathcal{T}_{01}}^T$  and  $V_{\mathcal{T}_{01}}$  share the same singular values, it follows that

$$\sqrt{\phi_{2S}}\|P_{\mathcal{W}} v\|_{\ell_2} \leq \|V_{\mathcal{T}_{01}}^T v\|_{\ell_2} / \sqrt{n}.$$

Applying this to  $v := Vh$  gives

$$\|P_{\mathcal{W}}Vh\|_{\ell_2} \leq (\phi_{2S})^{-1/2} \|V_{\mathcal{T}_{01}}^T Vh\|_{\ell_2} / \sqrt{n}. \quad (20)$$

We now divide  $\mathcal{T}_0^c$  into subsets of size  $S$ , where  $\mathcal{T}_1$  contains the indices of the  $S$  largest coefficients of  $h_{\mathcal{T}_0^c}$ ,  $\mathcal{T}_2$  contains the indices of the next  $S$  largest coefficients, and so on. Decompose  $P_{\mathcal{W}}Vh$  as

$$P_{\mathcal{W}}Vh = P_{\mathcal{W}}Vh_{\mathcal{T}_{01}} + \sum_{j \geq 2} P_{\mathcal{W}}Vh_{\mathcal{T}_j}.$$

By definition of  $\mathcal{W}$ , we have  $Vh_{\mathcal{T}_{01}} \in \mathcal{W}$  and  $P_{\mathcal{W}}Vh_{\mathcal{T}_{01}} = Vh_{\mathcal{T}_{01}}$ .

Since  $P_{\mathcal{W}}$  projects onto  $\mathcal{W}$ , there exists some  $c \in \mathbb{R}^L$  such that  $P_{\mathcal{W}}Vh_{\mathcal{T}_j} = \sum_{j \in \mathcal{T}_{01}} c_j V^j = Vc_{\mathcal{T}_{01}}$ , and

$$\|P_{\mathcal{W}}Vh_{\mathcal{T}_j}\|_{\ell_2}^2 = \langle P_{\mathcal{W}}Vh_{\mathcal{T}_j}, Vh_{\mathcal{T}_j} \rangle = \langle Vc_{\mathcal{T}_{01}}, Vh_{\mathcal{T}_j} \rangle.$$

By using the restricted orthogonality constant  $\theta_{S,2S}$  defined in Definition 2, we have

$$\begin{aligned} \langle Vc_{\mathcal{T}_{01}}, Vh_{\mathcal{T}_j} \rangle &\leq n\theta_{S,2S} \|c_{\mathcal{T}_{01}}\|_{\ell_2} \|h_{\mathcal{T}_j}\|_{\ell_2} \\ &\leq \frac{\sqrt{n}\theta_{S,2S}}{\sqrt{\phi_{2S}}} \|Vc_{\mathcal{T}_{01}}\|_{\ell_2} \|h_{\mathcal{T}_j}\|_{\ell_2} \\ &= \frac{\sqrt{n}\theta_{S,2S}}{\sqrt{\phi_{2S}}} \|P_{\mathcal{W}}Vh_{\mathcal{T}_j}\|_{\ell_2} \|h_{\mathcal{T}_j}\|_{\ell_2}. \end{aligned}$$

Thus,

$$\|P_{\mathcal{W}}Vh_{\mathcal{T}_j}\|_{\ell_2} \leq \frac{\sqrt{n}\theta_{S,2S}}{\sqrt{\phi_{2S}}} \|h_{\mathcal{T}_j}\|_{\ell_2}. \quad (21)$$

We now develop an upper bound for  $\sum_{j \geq 2} \|h_{\mathcal{T}_j}\|_{\ell_2}$  following [Candes et al. \(2005\)](#) and [Candes and Tao \(2007\)](#). By construction, for each component  $h_{\mathcal{T}_{j+1}}[i]$ ,

$$|h_{\mathcal{T}_{j+1}}[i]| \leq \|h_{\mathcal{T}_j}\|_{\ell_1} / S,$$

which implies

$$\|h_{\mathcal{T}_{j+1}}\|_{\ell_2}^2 \leq \|h_{\mathcal{T}_j}\|_{\ell_1}^2 / S,$$

and hence,

$$\sum_{j \geq 2} \|h_{\mathcal{T}_j}\|_{\ell_2} \leq S^{-1/2} \sum_{j \geq 1} \|h_{\mathcal{T}_j}\|_{\ell_1} = S^{-1/2} \|h_{\mathcal{T}_0^c}\|_{\ell_1}.$$

In summary,

$$\begin{aligned} \|P_{\mathcal{W}} V h\|_{\ell_2} &\geq \|P_{\mathcal{W}} V h_{\mathcal{T}_{01}}\|_{\ell_2} - \sum_{j \geq 2} \|P_{\mathcal{W}} V h_{\mathcal{T}_j}\|_{\ell_2} \\ &\geq \|V h_{\mathcal{T}_{01}}\|_{\ell_2} - \frac{\sqrt{n} \theta_{S,2S}}{\sqrt{\phi_{2S}}} S^{-1/2} \|h_{\mathcal{T}_0^c}\|_{\ell_1} \\ &\geq \sqrt{n \phi_{2S}} \|h_{\mathcal{T}_{01}}\|_{\ell_2} - \frac{\sqrt{n} \theta_{S,2S}}{\sqrt{\phi_{2S}}} S^{-1/2} \|h_{\mathcal{T}_0^c}\|_{\ell_1}. \end{aligned}$$

Combining this with (20) gives

$$\|h_{\mathcal{T}_{01}}\|_{\ell_2} \leq \frac{1}{n \phi_{2S}} \|V_{\mathcal{T}_{01}}^T V h\|_{\ell_2} + \frac{\theta_{S,2S}}{\phi_{2S} S^{1/2}} \|h_{\mathcal{T}_0^c}\|_{\ell_1},$$

which completes the proof.  $\square$

## 7.5 Lemma 5

**Lemma 5.** *Let  $\gamma = A\eta$ , where  $\eta$  is the coefficient vector under the selected basis  $\mathbf{B}$ . Suppose  $\gamma$  has at most  $S$  nonzero components, and let  $\mathcal{T}_0 = \{j : \gamma_j \neq 0\}$  denote its true support. Define  $V = XA^+$ , and assume  $V$  satisfies  $\phi_{2S} > \theta_{S,2S}$ . If*

$$\left\| \frac{1}{n} D^{-1} X^T (y - X\eta) \right\|_{\ell_\infty} \leq \lambda,$$

*then for  $\hat{\eta}$  obtained as the solution to (6), defining  $h = \hat{\gamma} - \gamma$  with  $\hat{\gamma} = A\hat{\eta}$  and letting  $\mathcal{T}_1$  be the  $S$  largest entries of  $h$  outside  $\mathcal{T}_0$ , we have*

$$\|h\|_{\ell_2} \leq \frac{\sqrt{2}}{n(\phi_{2S} - \theta_{S,2S})} \|V_{\mathcal{T}_{01}}^T V h\|_{\ell_2},$$

*where  $\mathcal{T}_{01} = \mathcal{T}_0 \cup \mathcal{T}_1$ .*

*Proof of Lemma 5.* Since  $\|h\|_{\ell_2}^2 = \|h_{\mathcal{T}_{01}}\|_{\ell_2}^2 + \|h_{\mathcal{T}_0^c}\|_{\ell_2}^2$ , combining this with inequality (16), we obtain

$$\|h\|_{\ell_2}^2 \leq \|h_{\mathcal{T}_{01}}\|_{\ell_2}^2 + \frac{1}{S} \|h_{\mathcal{T}_0^c}\|_{\ell_1}^2. \quad (22)$$

From Lemma 4, we have

$$\|h_{\mathcal{T}_{01}}\|_{\ell_2} \leq \frac{1}{n\phi_{2S}} \|V_{\mathcal{T}_{01}}^\top Vh\|_{\ell_2} + \frac{\theta_{S,2S}}{\phi_{2S}\sqrt{S}} \|h_{\mathcal{T}_0^c}\|_{\ell_1}.$$

In addition, we observe that

$$\|h_{\mathcal{T}_0}\|_{\ell_1} \leq \sqrt{S} \|h_{\mathcal{T}_0}\|_{\ell_2} \leq \sqrt{S} \|h_{\mathcal{T}_{01}}\|_{\ell_2}.$$

Substituting into the previous bound and using inequality (17), we get

$$\|h_{\mathcal{T}_{01}}\|_{\ell_2} \leq \frac{1}{n\phi_{2S}} \|V_{\mathcal{T}_{01}}^\top Vh\|_{\ell_2} + \frac{\theta_{S,2S}}{\phi_{2S}} \|h_{\mathcal{T}_{01}}\|_{\ell_2}.$$

Rearranging terms gives

$$\left(1 - \frac{\theta_{S,2S}}{\phi_{2S}}\right) \|h_{\mathcal{T}_{01}}\|_{\ell_2} \leq \frac{1}{n\phi_{2S}} \|V_{\mathcal{T}_{01}}^\top Vh\|_{\ell_2},$$

which implies

$$\|h_{\mathcal{T}_{01}}\|_{\ell_2} \leq \frac{1}{n(\phi_{2S} - \theta_{S,2S})} \|V_{\mathcal{T}_{01}}^\top Vh\|_{\ell_2}.$$

Now, combining (22) with (17), we have

$$\begin{aligned} \|h\|_{\ell_2}^2 &\leq \|h_{\mathcal{T}_{01}}\|_{\ell_2}^2 + \frac{1}{S} \|h_{\mathcal{T}_0^c}\|_{\ell_1}^2 \\ &\leq \|h_{\mathcal{T}_{01}}\|_{\ell_2}^2 + \frac{1}{S} \|h_{\mathcal{T}_0}\|_{\ell_1}^2 \\ &\leq 2\|h_{\mathcal{T}_{01}}\|_{\ell_2}^2, \end{aligned}$$

which yields

$$\|h\|_{\ell_2} \leq \frac{\sqrt{2}}{n(\phi_{2S} - \theta_{S,2S})} \|V_{\mathcal{T}_{01}}^\top Vh\|_{\ell_2}.$$

This completes the proof.  $\square$

## 7.6 Lemma 6

We now focus on the orthogonal decomposition. The following lemma bounds the difference between  $\hat{\eta}$  and  $\eta^*$ :

**Lemma 6.** Suppose  $\gamma^* = A\eta^*$  has at most  $S$  nonzero components and that  $\phi_{2S} > \theta_{S,2S}$  holds for  $V = XA^+$ . Let  $\hat{\gamma} = A\hat{\eta}$ , where  $\hat{\eta}$  is obtained by solving (6). If

$$\left\| \frac{1}{n} D^{-1} X^T (y - X\eta^*) \right\|_{\ell_\infty} \leq \lambda,$$

then

$$\|\hat{\gamma} - \gamma^*\|_{\ell_2} \leq \frac{4\sqrt{L}D_{\max}}{(\phi_{2S} - \theta_{S,2S})\sigma_{\min}(A)} \lambda\sqrt{S}, \quad (23)$$

and

$$\|\hat{\eta} - \eta^*\|_{\ell_2} \leq \frac{4\sqrt{L}D_{\max}}{(\phi_{2S} - \theta_{S,2S})\sigma_{\min}^2(A)} \lambda\sqrt{S}, \quad (24)$$

where  $D_{\max} = \max_{j=1,\dots,p} D_j$  and  $\sigma_{\min}(A)$  is the smallest singular value of  $A$ .

*Proof of Lemma 6.* Let  $h = \hat{\gamma} - \gamma^*$ , and let  $\mathcal{T}_0$  denote the support of  $\gamma^*$ , i.e.,

$$\mathcal{T}_0 = \{1 \leq j \leq L : \gamma_j^* \neq 0\},$$

so that  $|\mathcal{T}_0| \leq S$ . Let  $\mathcal{T}_1$  be the index set of the  $S$  largest entries of  $h$  outside  $\mathcal{T}_0$ , and define  $\mathcal{T}_{01} = \mathcal{T}_0 \cup \mathcal{T}_1$ .

From Lemma 5, we have

$$\|h\|_{\ell_2} \leq \frac{\sqrt{2}}{n(\phi_{2S} - \theta_{S,2S})} \|V_{\mathcal{T}_{01}}^\top Vh\|_{\ell_2}. \quad (25)$$

To bound  $\|V_{\mathcal{T}_{01}}^\top Vh\|_{\ell_2}$ , note that

$$\|V_{\mathcal{T}_{01}}^\top Vh\|_{\ell_2} \leq \sqrt{2S} \cdot \|V^\top Vh\|_{\ell_\infty}.$$

Combining this with (25), inequality (18), and bound (19), we obtain

$$\begin{aligned} \|h\|_{\ell_2} &\leq \frac{\sqrt{2}}{n(\phi_{2S} - \theta_{S,2S})} \cdot \sqrt{2S} \cdot \|V^\top Vh\|_{\ell_\infty} \\ &\leq \frac{2\sqrt{L}D_{\max}}{(\phi_{2S} - \theta_{S,2S})\sigma_{\min}(A)} \sqrt{S} \left\| \frac{1}{n} D^{-1} X^\top Vh \right\|_{\ell_\infty} \\ &\leq \frac{4\sqrt{L}D_{\max}}{(\phi_{2S} - \theta_{S,2S})\sigma_{\min}(A)} \lambda\sqrt{S}. \end{aligned}$$

Finally, since  $\hat{\eta} - \eta^* = A^+h$ , we have

$$\|\hat{\eta} - \eta^*\|_{\ell_2} = \|A^+h\|_{\ell_2} \leq \frac{\|h\|_{\ell_2}}{\sigma_{\min}(A)},$$

which establishes the bound in (24).  $\square$

## 7.7 Proof of Theorem 1

*Proof of Theorem 1.* From Lemmas 1 and 6, we know that inequalities (23) and (24) hold simultaneously with probability at least  $1 - p^{1-C^2/2}$ , for some constant  $C > \sqrt{2}$  and

$$\lambda = C\sigma\sqrt{\frac{\log p}{n}} + M\omega_{\mathbf{B}}.$$

By the definition of the  $L^2(\Omega)$  norm, the triangle inequality, and the Cauchy–Schwarz inequality, we obtain

$$\begin{aligned} \|\hat{\beta} - \beta\|_{L^2(\Omega)} &\leq \left\| \sum_{j=1}^p (\hat{\eta}_j - \eta_j^*) b_j(t, s) \right\|_{L^2(\Omega)} + \|e\|_{L^2(\Omega)} \\ &\leq \sqrt{\sum_{j=1}^p \left( \iint_{\Omega} b_j^2(t, s) dt ds \right)} \cdot \|\hat{\eta} - \eta^*\|_{\ell_2} + \omega_{\mathbf{B}}. \end{aligned} \quad (26)$$

Inequality (9) then follows directly from (26) and (24).

To bound the prediction error  $\|\hat{f} - f\|_n$ , let  $f = X\eta^* + v$ , where  $v$  is defined in (14), and  $\hat{f} = X\hat{\eta}$ . By the triangle inequality,

$$\|\hat{f} - f\|_n \leq \frac{1}{\sqrt{n}} \|X(\hat{\eta} - \eta^*)\|_{\ell_2} + \|v\|_n,$$

where, from Lemma 1,

$$\|v\|_n = \frac{1}{\sqrt{n}} \|v\|_{\ell_2} \leq \|v\|_{\ell_1} \leq M\omega_{\mathbf{B}}.$$

To bound the first term, note that from Lemma 3, we have

$$\frac{1}{n} \|V^\top Vh\|_{\ell_\infty} \leq \frac{\sqrt{L}D_{\max}}{\sigma_{\min}(A)} \left\| \frac{1}{n} D^{-1} X^\top Vh \right\|_{\ell_\infty},$$

and

$$\left\| \frac{1}{n} D^{-1} X^\top V h \right\|_{\ell_\infty} \leq 2\lambda.$$

Combining these with (23), we get

$$\begin{aligned} \frac{1}{n} \|X(\hat{\eta} - \eta^*)\|_{\ell_2}^2 &= \frac{1}{n} h^\top V^\top V h \\ &\leq \frac{1}{n} \|V^\top V h\|_{\ell_\infty} \cdot \|h\|_{\ell_1} \\ &\leq \frac{\sqrt{L} D_{\max}}{\sigma_{\min}(A)} \cdot \left\| \frac{1}{n} D^{-1} X^\top V h \right\|_{\ell_\infty} \cdot 2 \|h_{\mathcal{T}_0}\|_{\ell_1} \\ &\leq \frac{4\sqrt{L} D_{\max}}{\sigma_{\min}(A)} \lambda \sqrt{S} \cdot \|h\|_{\ell_2} \\ &\leq \frac{16L D_{\max}^2}{(\phi_{2S} - \theta_{S,2S}) \sigma_{\min}^2(A)} \lambda^2 S. \end{aligned}$$

Taking square roots yields

$$\frac{1}{\sqrt{n}} \|X(\hat{\eta} - \eta^*)\|_{\ell_2} \leq \frac{4\sqrt{L} D_{\max}}{\sqrt{\phi_{2S} - \theta_{S,2S}} \sigma_{\min}(A)} \lambda \sqrt{S}.$$

Therefore, the prediction error is bounded as

$$\|\hat{f} - f\|_n \leq \frac{4\sqrt{L} D_{\max}}{\sqrt{\phi_{2S} - \theta_{S,2S}} \sigma_{\min}(A)} \lambda \sqrt{S} + M\omega_{\mathbf{B}},$$

which establishes inequality (10) and completes the proof.  $\square$

## 8 Proof of Theorem 2

Before presenting the proof of Theorem 2, we first introduce Lemma 7 and 8. These results serve as key building blocks for the proof of Theorem 2.

### 8.1 Lemma 7

**Lemma 7.** *Suppose  $\gamma^* = A\eta^*$  has at most  $S$  nonzero components and that  $\kappa_1(S) > 0$  holds for  $V = XA^+$ . Let  $\hat{\gamma} = A\hat{\eta}$ , where  $\hat{\eta}$  is obtained by solving (6). If*

$$\left\| \frac{1}{n} D^{-1} X^T (y - X\eta^*) \right\|_{\ell_\infty} \leq \lambda,$$

then

$$\|\hat{\gamma} - \gamma^*\|_{\ell_1} \leq \frac{8\sqrt{L}D_{\max}}{\kappa_1^2(S)\sigma_{\min}(A)}\lambda S, \quad (27)$$

and

$$\frac{1}{n}\|V(\hat{\gamma} - \gamma^*)\|_{\ell_2}^2 \leq \frac{16LD_{\max}^2}{\kappa_1^2(S)\sigma_{\min}^2(A)}\lambda^2 S, \quad (28)$$

where  $D_{\max} = \max_{j=1,\dots,p} D_j$  and  $\sigma_{\min}(A)$  is the smallest singular value of  $A$ .

*Proof of Lemma 7.* By using (18) and (19), we bound

$$\begin{aligned} \frac{1}{n}\|Vh\|_{\ell_2}^2 &= \frac{1}{n}h^\top V^\top Vh \\ &\leq \frac{1}{n}\|V^\top Vh\|_{\ell_\infty}\|h\|_{\ell_1} \\ &\leq \frac{\sqrt{L}D_{\max}}{\sigma_{\min}(A)}\left\|\frac{1}{n}D^{-1}X^\top Vh\right\|_{\ell_\infty}\|h\|_{\ell_1} \\ &\leq \frac{2\sqrt{L}D_{\max}}{\sigma_{\min}(A)}\lambda\|h\|_{\ell_1} \\ &\leq \frac{2\sqrt{L}D_{\max}}{\sigma_{\min}(A)}\lambda\left(\|h_{\mathcal{T}_0}\|_{\ell_1} + \|h_{\mathcal{T}_0^c}\|_{\ell_1}\right) \\ &\leq \frac{4\sqrt{L}D_{\max}}{\sigma_{\min}(A)}\lambda\|h_{\mathcal{T}_0}\|_{\ell_1}. \end{aligned}$$

Since  $\|h_{\mathcal{T}_0}\|_{\ell_1} \leq \sqrt{S}\|h_{\mathcal{T}_0}\|_{\ell_2}$ , we obtain

$$\frac{1}{n}\|Vh\|_{\ell_2}^2 \leq \frac{4\sqrt{L}D_{\max}}{\sigma_{\min}(A)}\lambda\sqrt{S}\|h_{\mathcal{T}_0}\|_{\ell_2}. \quad (29)$$

Since  $\kappa_1(S) > 0$ , by Definition 3 (restricted eigenvalue condition), we also have

$$\frac{1}{n}\|Vh\|_{\ell_2}^2 \geq \kappa_1^2(S)\|h_{\mathcal{T}_0}\|_{\ell_2}^2.$$

Combining this with (29) yields

$$\|h_{\mathcal{T}_0}\|_{\ell_2} \leq \frac{4\sqrt{L}D_{\max}}{\kappa_1^2(S)\sigma_{\min}(A)}\lambda\sqrt{S}. \quad (30)$$



Therefore,

$$\begin{aligned}
\|h\|_{\ell_1} &= \|h_{\mathcal{T}_0}\|_{\ell_1} + \|h_{\mathcal{T}_0^c}\|_{\ell_1} \\
&\leq 2\|h_{\mathcal{T}_0}\|_{\ell_1} \\
&\leq 2\sqrt{S}\|h_{\mathcal{T}_0}\|_{\ell_2} \\
&\leq \frac{8\sqrt{L}D_{\max}}{\kappa_1^2(S)\sigma_{\min}(A)}\lambda S,
\end{aligned}$$

which proves inequality (27). Furthermore, combining (30) with (29) establishes inequality (28).  $\square$

## 8.2 Lemma 8

**Lemma 8.** *Assume all the conditions in Lemma 7. If  $\kappa_2(S, S) > 0$  is satisfied, then we have*

$$\|\hat{\gamma} - \gamma^*\|_{\ell_2} \leq \frac{8\sqrt{L}D_{\max}}{\kappa_2^2(S, S)\sigma_{\min}(A)}\lambda\sqrt{S}, \quad (31)$$

and

$$\|\hat{\eta} - \eta^*\|_{\ell_2} \leq \frac{8\sqrt{L}D_{\max}}{\kappa_2^2(S, S)\sigma_{\min}^2(A)}\lambda\sqrt{S}. \quad (32)$$

*Proof of Lemma 8.* From inequality (29), we have

$$\frac{1}{n}\|Vh\|_{\ell_2}^2 \leq \frac{4\sqrt{L}D_{\max}}{\sigma_{\min}(A)}\lambda\sqrt{S}\|h_{\mathcal{T}_{01}}\|_{\ell_2}.$$

Since  $\kappa_2(S, S) > 0$ , by Definition 4, the restricted eigenvalue condition implies

$$\frac{1}{n}\|Vh\|_{\ell_2}^2 \geq \kappa_2^2(S, S)\|h_{\mathcal{T}_{01}}\|_{\ell_2}^2.$$

Combining the two inequalities yields

$$\|h_{\mathcal{T}_{01}}\|_{\ell_2} \leq \frac{4\sqrt{L}D_{\max}}{\kappa_2^2(S, S)\sigma_{\min}(A)}\lambda\sqrt{S}.$$

From Lemma 2, specifically inequalities (16) and (17), we have

$$\|h_{\mathcal{T}_{01}^c}\|_{\ell_2} \leq \frac{1}{\sqrt{S}}\|h_{\mathcal{T}_0^c}\|_{\ell_1} \leq \|h_{\mathcal{T}_0}\|_{\ell_2} \leq \|h_{\mathcal{T}_{01}}\|_{\ell_2},$$

and thus,

$$\|h\|_{\ell_2} \leq \|h_{\mathcal{T}_{01}^c}\|_{\ell_2} + \|h_{\mathcal{T}_{01}}\|_{\ell_2} \leq 2\|h_{\mathcal{T}_{01}}\|_{\ell_2}.$$

Therefore,

$$\|h\|_{\ell_2} \leq \frac{8\sqrt{L}D_{\max}}{\kappa_2^2(S, S)\sigma_{\min}(A)}\lambda\sqrt{S},$$

which proves inequality (31).

Finally, since  $\hat{\eta} - \eta^* = A^+h$ , we have

$$\|\hat{\eta} - \eta^*\|_{\ell_2} = \|A^+h\|_{\ell_2} \leq \frac{1}{\sigma_{\min}(A)}\|h\|_{\ell_2},$$

which establishes inequality (32). □

### 8.3 Proof of Theorem 2

*Proof of Theorem 2.* From Lemmas 1 and 7, we know that inequalities (27) and (28) hold simultaneously with probability at least  $1 - p^{1-C^2/2}$ , for some constant  $C > \sqrt{2}$  and

$$\lambda = C\sigma\sqrt{\frac{\log p}{n}} + M\omega_{\mathbf{B}}.$$

Observe that

$$\|\hat{\eta} - \eta^*\|_{\ell_2} \leq \frac{\|\hat{\gamma} - \gamma^*\|_{\ell_2}}{\sigma_{\min}(A)} \leq \frac{\|\hat{\gamma} - \gamma^*\|_{\ell_1}}{\sigma_{\min}(A)}.$$

Combining this with (27) and inequality (26) establishes the bound in (11).

Now consider prediction error. Similar from the proof of Theorem 1, we have

$$\|\hat{f} - f\|_n \leq \frac{1}{\sqrt{n}}\|X(\hat{\eta} - \eta^*)\|_{\ell_2} + \|v\|_n$$

and

$$\|v\|_n \leq M\omega_{\mathbf{B}}.$$

Also, from Lemma 7, we have

$$\begin{aligned}\frac{1}{n}\|X(\hat{\eta} - \eta^*)\|_{\ell_2}^2 &= \frac{1}{n}\|V(\hat{\gamma} - \gamma^*)\|_{\ell_2}^2 \\ &\leq \frac{16LD_{\max}^2}{\kappa_1^2(S)\sigma_{\min}^2(A)}\lambda^2 S,\end{aligned}$$

which implies

$$\frac{1}{\sqrt{n}}\|X(\hat{\eta} - \eta^*)\|_{\ell_2} \leq \frac{4\sqrt{L}D_{\max}}{\kappa_1(S)\sigma_{\min}(A)}\lambda\sqrt{S},$$

and this yields the prediction bound in (12).

Finally, if the stronger restricted eigenvalue condition  $\kappa_2(S, S) > 0$  holds, then inequality (13) follows directly from (26) and Lemma 8.  $\square$

## 9 Additional Discussions on the Restricted Eigenvalue Conditions

### 9.1 Sufficient Condition for the RE Conditions

The following Lemma 9 states that (A4) is a sufficient condition for both (A5) and (A6).

**Lemma 9** (cf. Lemma 4.1 in Bickel et al. (2009)). *Suppose that  $\phi_{2S} - \theta_{S,2S} > 0$ . Then both  $\kappa_1(S) > 0$  and  $\kappa_2(S, S) > 0$ .*

*Proof of Lemma 9.* Let  $h \in \mathbb{R}^L$  be any vector satisfies that  $\|h_{\mathcal{T}_0^c}\|_{\ell_1} \leq \|h_{\mathcal{T}_0}\|_{\ell_1}$ . Following the construction used in the proof of Lemma 4, we partition  $\mathcal{T}_0^c$  into disjoint subsets of size at most  $S$ , i.e.,

$$\mathcal{T}_0^c = \bigcup_{k=1}^K \mathcal{T}_k,$$

where  $|\mathcal{T}_k| = S$  for  $k = 1, \dots, K-1$ , and  $|\mathcal{T}_K| \leq S$ . The sets  $\mathcal{T}_k$  are defined recursively:  $\mathcal{T}_1$  contains the indices of the  $S$  largest (in magnitude) entries of  $h$  outside  $\mathcal{T}_0$ ,  $\mathcal{T}_2$  the next largest  $S$ , and so on. Define  $\mathcal{T}_{01} = \mathcal{T}_0 \cup \mathcal{T}_1$ .

Let  $\mathcal{W} \subset \mathbb{R}^n$  be the linear span of  $\{V^j : j \in \mathcal{T}_{01}\}$ , and let  $P_{\mathcal{W}}$  denote the orthogonal projection onto  $\mathcal{W}$ . From inequality (21), we have

$$\frac{\|P_{\mathcal{W}}Vh_{\mathcal{T}_k}\|_{\ell_2}}{\sqrt{n}} \leq \frac{\theta_{S,2S}}{\sqrt{\phi_{2S}}} \|h_{\mathcal{T}_k}\|_{\ell_2}, \quad \text{for } k \geq 2.$$

Now consider the lower bound:

$$\begin{aligned} \|P_{\mathcal{W}}Vh\|_{\ell_2} &\geq \|P_{\mathcal{W}}Vh_{\mathcal{T}_{01}}\|_{\ell_2} - \left\| \sum_{k=2}^K P_{\mathcal{W}}Vh_{\mathcal{T}_k} \right\|_{\ell_2} \\ &= \|Vh_{\mathcal{T}_{01}}\|_{\ell_2} - \sum_{k=2}^K \|P_{\mathcal{W}}Vh_{\mathcal{T}_k}\|_{\ell_2}, \end{aligned}$$

where we used the fact that  $P_{\mathcal{W}}Vh_{\mathcal{T}_{01}} = Vh_{\mathcal{T}_{01}}$  by construction.

Therefore,

$$\frac{\|P_{\mathcal{W}}Vh\|_{\ell_2}}{\sqrt{n}} \geq \sqrt{\phi_{2S}} \|h_{\mathcal{T}_{01}}\|_{\ell_2} - \sum_{k=2}^K \frac{\theta_{S,2S}}{\sqrt{\phi_{2S}}} \|h_{\mathcal{T}_k}\|_{\ell_2}.$$

Next, we observe that

$$\sum_{k=2}^K \|h_{\mathcal{T}_k}\|_{\ell_2} \leq \frac{1}{\sqrt{S}} \|h_{\mathcal{T}_0^c}\|_{\ell_1} \leq \frac{1}{\sqrt{S}} \|h_{\mathcal{T}_0}\|_{\ell_1} \leq \|h_{\mathcal{T}_0}\|_{\ell_2} \leq \|h_{\mathcal{T}_{01}}\|_{\ell_2}.$$

Substituting this bound yields

$$\frac{\|P_{\mathcal{W}}Vh\|_{\ell_2}}{\sqrt{n}} \geq \sqrt{\phi_{2S}} \left( 1 - \frac{\theta_{S,2S}}{\phi_{2S}} \right) \|h_{\mathcal{T}_{01}}\|_{\ell_2}.$$

Finally, since projections cannot increase norm, we have

$$\frac{\|Vh\|_{\ell_2}}{\sqrt{n}} \geq \frac{\|P_{\mathcal{W}}Vh\|_{\ell_2}}{\sqrt{n}},$$

and therefore,

$$\frac{\|Vh\|_{\ell_2}}{\sqrt{n}} \geq \sqrt{\phi_{2S}} \left( 1 - \frac{\theta_{S,2S}}{\phi_{2S}} \right) \|h_{\mathcal{T}_{01}}\|_{\ell_2}.$$

This inequality verifies the restricted eigenvalue conditions in Definitions 3 and 4, and hence

$\kappa_1(S) > 0$  and  $\kappa_2(S, S) > 0$ . □

## 9.2 Illustrative Example for the RE Conditions

Suppose we observe a  $2 \times 2$  grid over the predictor surface. On this grid, we adopt the piecewise constant basis, which gives  $p = 4$  and leads to a basis matrix  $B = I_4$ . Set the sparsity-smoothness trade-off parameter to  $w = 1$ , and let the difference orders in both directions be  $d_1 = d_2 = 1$ . Under this setting, the matrix  $A$  becomes

$$A = \begin{bmatrix} 1 & 0 & 0 & 0 \\ 0 & 1 & 0 & 0 \\ 0 & 0 & 1 & 0 \\ 0 & 0 & 0 & 1 \\ 1 & -1 & -1 & 1 \end{bmatrix}.$$

We generate a matrix  $X \in \mathbb{R}^{4 \times 4}$  with each entry independently drawn from  $\mathcal{N}(0, 1)$ :

$$X = \begin{bmatrix} 0.7533 & -2.2169 & -1.7922 & 0.8647 \\ 2.0144 & 0.7584 & -0.0420 & -1.7202 \\ -0.3551 & -1.3062 & 2.1500 & 0.1341 \\ 2.0282 & -0.8025 & -1.7702 & -0.0758 \end{bmatrix}.$$

This yields the matrix  $V = XA^+$ :

$$V = \begin{bmatrix} -0.3721 & -1.0915 & -0.6668 & -0.2608 & 1.1254 \\ 2.0988 & 0.6740 & -0.1265 & -1.6357 & -0.0844 \\ -0.1422 & -1.5192 & 1.9371 & 0.3471 & -0.2130 \\ 1.1231 & 0.1025 & -0.8652 & -0.9808 & 0.9050 \end{bmatrix}.$$

Next, we generate a random vector  $h \in \mathbb{R}^5$  such that  $\|h_{\mathcal{T}_0^c}\|_{\ell_1} \leq \|h_{\mathcal{T}_0}\|_{\ell_1}$ , where  $|\mathcal{T}_0| = 1$ .

Let  $\mathcal{T}_1$  be the index corresponding to the largest (in magnitude) entry of  $h$  outside  $\mathcal{T}_0$ , and define  $\mathcal{T}_{01} = \mathcal{T}_0 \cup \mathcal{T}_1$ . We then compute the two ratios:

$$\frac{\|Vh\|_{\ell_2}}{\sqrt{4}\|h_{\mathcal{T}_0}\|_{\ell_2}} \quad \text{and} \quad \frac{\|Vh\|_{\ell_2}}{\sqrt{4}\|h_{\mathcal{T}_{01}}\|_{\ell_2}}.$$

This process is repeated 10,000 times, and the smallest values are recorded. The resulting numerical estimates are  $\kappa_1(1) \approx 0.3051$  and  $\kappa_2(1, 1) \approx 0.2594$ .